A mesoscopic simulation method for predicting the rheology of semi-dilute wormlike micellar solutions

Weizhong Zou and Ronald G. Larson[a)]

Department of Chemical Engineering, University of Michigan, Ann Arbor, Michigan 48105

(Received 3 December 2013; final revision received 4 March 2014; published 28 March 2014)

Synopsis

We present a fast "pointer" simulation method that extends the model of Cates and coworkers for the rheology of entangled wormlike micelles. Our method includes not only reptation, breakage/rejoining, contour length fluctuations, and Rouse modes, which were included in Cates' model, but also constraint release, bending modes, and a cross-over to the tight entanglement regime, which had not been previously considered. Our method also contains correlations in micelle length across multiple breakage/rejoining cycles, not included in previous approaches. Our method uses "pointers" that track the ends of unrelaxed regions along each micelle, thereby allowing efficient simulations of relaxation dynamics for ensembles containing thousands of micelles, to obtain accurate results without preaveraging or neglecting correlations. A modified genetic algorithm is applied to transform the simulation data from the time to the frequency domain. The method can span several regimes of behavior depending on the relative rates of reptation, contour length fluctuations, breakage/rejoining, and high frequency modes and is suitable for predicting the rheological behavior of experimental solutions for wormlike micelles. This new simulation method allows extraction of multiple micellar parameters simultaneously by fitting experimental rheology data across the entire available frequency range. Values of average micelle length and breakage rate thereby obtained can be an order of magnitude different from previous estimates based on "local" frequency dependencies predicted by Cates' model. These differences are due to more complete physics included in our method and the fitting of G' and G'' data across the entire frequency range. We also provide quantitative relationships between these parameters and rheological behaviors that improve on previous simple scaling results. © *2014 The Society of Rheology*.
[http://dx.doi.org/10.1122/1.4868875]

I. INTRODUCTION

Surfactant solutions with various self-assembled structures have been intensively studied in recent years. Such structures include small spheroidal micelles, long wormlike micelles [Lequeux (1996)], ellipsoids, bilayers [Nagarajan (1989)], and ordered phases that depend on type and concentration of salt [Candau *et al*. (1993); Wang and Larson (2009)], surfactant [Hassan *et al*. (1998); Gomez *et al*. (2010)], temperature, and solvent [Bruce *et al*. (2002); Jusufi *et al*. (2008)]. Above the critical micelle concentration (CMC), surfactant molecules aggregate to form equilibrium spherical micelles. While

[a)]Electronic mail: rlarson@umich.edu

changes in equilibrium structure are induced in a variety of ways [Michels and Waton (2003); Terech *et al*. (1992); Helgeson *et al*. (2010); Oelschlaeger *et al*. (2009)], a transition from spheroid to wormlike micelles often occurs with increasing salt concentration, and further increases can result in micelle branching and network formation [Ilgenfritz *et al*. (2004)]. With the widespread use of micelles and surfactant solutions [Rosen (1989); Siriwatwechakul *et al*. (2004)], extensively attention has been paid to determining the properties of micelle-solvent systems using computer simulations [Shang *et al*. (2009)], theoretical modeling [Cates and Candau (1990)], or advanced experimental techniques [Kuperkar *et al*. (2008)].

It has long been noted that the rheological properties of wormlike micellar solutions have similarities to those of long polymers [Candau *et al*. (1993); Cates and Candau (1990)]. A number of theories that exploit those similarities have been developed [Wittmer *et al*. (1998); Grmela *et al*. (2010); Rothstein (2003)] that treat wormlike micelles as living/equilibrium polymers, which incessantly break and rejoin in thermal equilibrium. Using the tube concept for entangled polymer, Cates and coworkers [Cates and Candau (1990); Cates (1987); Turner and Cates (1991)] developed a model that qualitatively or semi-quantitatively predicts the rheology of wormlike micellar solutions and allows properties of micelles, such as their length and rate of breakage, to be inferred from rheology. Despite its successes, there remain gaps [Lequeux (1992); van der Schoot and Wittmer (1999); Larson (2012)] in the theory, as discussed in this paper. Meanwhile, over the past twenty years since the introduction of Cates' model, many improvements have been developed for more accurate description of the rheology of entangled polymer solutions and melts [Dealy and Larson (2005)]. It is, therefore, time to consider if those new developments might be exploited to improve upon Cates' model for wormlike micelles.

In this paper, we describe a novel simulation method for extending Cates' model by including additional physics known to be important in entangled polymer solutions but neglected in the earlier theories. In what follows, Sec. II defines needed terminology, Sec. III focuses on the theoretical development of our method, starting with a brief review of Cates' model, followed by descriptions of currently understood polymer relaxation mechanisms, and ending with the mathematics underlying our simulation method. Section IV describes the computational part of our method in detail, including the pointer algorithm and the genetic algorithm (GA) that converts results from the time to the frequency domain. After several simulation tests in Sec. V, Sec. VI contains analyses and discussions of relaxation mechanisms, parameters, and compares results from our method with those from Cates' model using two different procedures. At the end of Sec. VI, our simulation method is applied to experimental data to estimate characteristic parameters of some experimental semi-dilute micellar solutions. Conclusions and future work are presented in Sec. VII.

II. DEFINITIONS

To avoid confusion, we first present definitions of following parameters.

A. L, L_t, $\langle L \rangle$, and $\langle L_t \rangle$

L is the (contour) length of a specific micelle, while L_t is the corresponding tube length. The relationship between tube length and micelle (contour) length can be found in Sec. III. Here, $\langle \cdot \rangle$ denotes an ensemble average over the distribution of micelle lengths or tube lengths.

B. τ_{rep} and $\bar{\tau}_{rep}$

Here, τ_{rep} is the characteristic reptation time for a micelle of length L and curvilinear diffusion coefficient D_c, given in Eq. (12). $\bar{\tau}_{rep}$ is the value of τ_{rep} for a micelle of average length $\langle L \rangle$. In general, an overbar means that the given micelle parameter is evaluated for a micelle of length $\langle L \rangle$.

C. a and d

Here, a is the tube diameter, while d is the micelle diameter.

D. b_K and l_p

The Kuhn length (b_K) is defined using

$$\langle R^2 \rangle_0 = N_K b_K^2 = b_K L = a L_t, \tag{1}$$

where $\langle R^2 \rangle_0$ is the mean-square end-to-end distance of a micelle and N_K is the number of Kuhn steps in the micelle. Note that the persistence length (l_p) is equal to $b_K/2$.

E. Z and Z_t

Z is the number of entanglements for a micelle with length L, while Z_t donates the ratio of micelle tube length to the entanglement length (l_e)

$$Z \equiv \frac{L}{l_e}, \quad Z_t \equiv \frac{L_t}{l_e}. \tag{2}$$

Here, the entanglement length l_e is the length of micelle per entanglement. We discuss later how to estimate this.

F. ξ, ς, ζ, and ζ_K

Here, ξ is the excluded volume screening length (or blob/mesh size), which has units of length and in a good solvent is related to the persistence length and entanglement length by [Cates (1988); Granek and Cates (1992)]

$$\xi = l_p^{0.4} l_e^{0.6}. \tag{3}$$

The dimensionless breakage rate ς is a ratio of two time constants, namely, the breakage time to the reptation time, given in Eq. (6). The drag coefficient per unit micelle length ζ is given by [Morse (1998b)]

$$\zeta = \frac{2\pi\eta_s}{\ln(\xi/d)}. \tag{4}$$

Finally, ζ_K is the drag coefficient per micelle Kuhn step with units of force per unit velocity, which is related to ζ by Eq. (5). Note that both of these drag coefficients are used in this paper

$$N_K \zeta_K = \zeta L. \tag{5}$$

G. $\bar{\tau}_{br}, \tau, \tau_R$, and τ_e

Here, $\bar{\tau}_{br}$ is the average micelle breakage time and is related to the average micelle reptation time ($\bar{\tau}_{rep}$) by the dimensionless breakage rate ς

$$\varsigma \equiv \frac{\bar{\tau}_{br}}{\bar{\tau}_{rep}}. \tag{6}$$

We take τ to be the stress relaxation time, defined as the inverse of the crossover frequency (ω_{cross}) of the storage modulus (G') with the loss modulus (G''). τ_R is Rouse rotational time given by

$$\tau_R = \frac{\zeta_K N_K^2 b_K^2}{3\pi^2 k_B T} \quad . \tag{7}$$

Here, again, ζ_K is drag coefficient per Kuhn step, k_B is Boltzmann's constant, and T is the temperature. The equilibration time (τ_e) is the Rouse time of a chain segment between entanglements. For monodisperse chains, the relationships [Larson *et al*. (2003)] among τ_{rep}, τ_e, and τ_R are given by

$$\tau_{rep} = 3Z\tau_R = 3Z^3\tau_e. \tag{8}$$

All these time constants will be used in this paper.

H. α_e

The semi-flexibility factor α_e is defined as the ratio of entanglement length to persistence length

$$\alpha_e \equiv \frac{l_e}{l_p}. \tag{9}$$

Note in the early work of Cates (1987), the parameter $\alpha(\equiv \bar{Z}^{-1})$ was introduced to approximate the influence of contour length fluctuations (CLFs), which were called "breathing fluctuations."

III. THEORY

Here, we first briefly review the tube model and reptation theory.

A. Tube model and reptation theory

In the well-entangled regime, the motion of an individual chainlike molecule is confined to a "tube"-like region by topological constraints imposed by its neighbors [Dealy and Larson (2005); Doi and Edwards (1986)]. The tube length is no greater than the chain length and the so-called tube diameter (a) is the length of a tube segment or a "tube Kuhn length." For the so-called "loosely" and "tightly entangled" regimes (defined shortly), a is determined by the entanglement length (l_e)

$$\text{Loose entanglements: } a^2 = N_e b_K^2 = 2 l_e l_p, \tag{10a}$$

$$\text{Tight entanglements: } a = l_e. \tag{10b}$$

Here, N_e is the number of Kuhn steps in a single tube segment. By combining Eq. (1) with Eq. (10a), we can obtain an important relationship involving tube length (L_t) and chain length (L) for the loosely entangled regime

$$l_e L_t = aL. \tag{11}$$

In the tube, a "chain" can alter its conformation by diffusing along the curvilinear path of the tube, which is a process known as "reptation" [de Gennes (1979)]. Any part of the chain that diffuses out of the tube instantly achieves an equilibrium conformation. (While this is not strictly true in the tight entanglement limit, wormlike micelles are typically close enough to being loosely entangled, and are long enough, that this approximation is a reasonable one even for tightly entangled micelles.) The reptation time and curvilinear diffusion coefficient D_c of a chain with length L are given by

$$\tau_{rep} = \frac{L_t^2}{\pi^2 D_c}, \quad D_c \equiv \frac{D_0}{L}, \quad D_0 = \frac{k_B T}{\zeta}, \tag{12}$$

where D_0 and ζ are the diffusivity and drag coefficient per unit length of chain, respectively.

With these parameters, the fraction of tube remaining occupied at a time t after a small step deformation, which is proportional to the fraction of remaining stress (μ), for pure reptation, is

$$\mu(t) = \frac{8}{\pi^2} \sum_{p=odd} p^{-2} exp\left(\frac{-tp^2}{\tau_{rep}}\right). \tag{13}$$

The detailed derivation can be found in Doi and Edwards (1986). However, Eq. (13) is only accurate for monodisperse chains, and this formula assumes a fixed contour length and neglect of other high frequency motions [Likhtman and McLeish (2002)].

B. Cates' model

In 1987, Cates put forward a model to address the "living" feature (breakage/rejoining) of micelle chains within the framework of tube model and reptation dynamics. The model successfully explained the nearly single-exponential shape of the stress relaxation function $\mu(t)$ for simple surfactants that form wormlike micelles such as cetyltrimethylammonium (CTA) surfactants [Turner and Cates (1991); Lequeux (1992)]. The original Cates' model rests on several assumptions [Cates (1987); Candau *et al*. (1989)], namely, (i) Micelles break with a uniform probability per unit length. The corresponding average breakage time ($\bar{\tau}_{br}$) is defined as the lifetime of a micelle with average length $\langle L \rangle$

$$\bar{\tau}_{br} = \frac{1}{k\langle L \rangle}, \tag{14}$$

where k is the breakage rate per unit length. (ii) Successive breakage and rejoining events are uncorrelated, and breakage is unimicellar while rejoining is bimicellar. (iii) Micelle relaxation occurs through reptation. (iv) Tube rearrangement or constraint release (CR) is neglected.

Consistent with the above assumptions, the equilibrium statistical mechanics, based on a free energy containing translational entropy, and an end-cap free energy that is independent of micelle length, yields the following micellar length distribution [Cates (1987)]:

$$N(L) = \frac{k}{k'} \exp\left(\frac{-L}{\langle L \rangle}\right), \quad \frac{k}{k'} = \frac{\rho}{2\langle L \rangle^2}, \tag{15a}$$

$$\rho = \int_0^\infty LN(L)dL. \tag{15b}$$

Here, $N(L)dL$ is the number density of micelles with length $L \pm dL/2$, ρ is the contour length of micelles per unit volume of solution, k is the rate constant for breakage, and k' is the rate constant for rejoining. See the original paper of Cates (1987) for details.

According to assumptions (iii) and (iv), the original Cates' model limits relaxation mechanisms of micelles to reptation assisted by breakage and rejoining. Note that by breaking, new ends are created, which helps to accelerate relaxation by reptation. For $\bar{\tau}_{br} \gg \bar{\tau}_{rep}$, breakage is slow compared to reptation, and the relaxation is dominated by reptation of polydisperse micelles; for $\bar{\tau}_{br} \ll \bar{\tau}_{rep}$, the relaxation is controlled by the interplay of breakage/rejoining with reptation, which yields a nearly monoexponential decay with stress relaxation time (τ)

$$\tau \sim \bar{\tau}_{rep}\varsigma^{0.5}, \quad \varsigma = \frac{\bar{\tau}_{br}}{\bar{\tau}_{rep}} \ll 1 \ . \tag{16}$$

Thus, when Eq. (16) applies, the approximate single exponential relaxation produces a nearly semicircular "Cole-Cole" cross-plot of loss modulus (G'') against storage modulus (G'). Nevertheless, in experiments, an increase of G'' is always observed after a minimum is reached on the right side (i.e., the high frequency side) of the Cole-Cole plot [Granek (1994)], implying that additional relaxation mechanisms are present at high frequencies. Cates and coworkers, therefore, added breathing fluctuations or CLFs, which describe time dependent changes in the length of the tube contour.

The timescale of these breathing fluctuations relative to reptation is set by $\bar{Z}$, the number of entanglements for a micelle with average length $\langle L \rangle$, according to

$$\bar{\tau}_{breath} \sim \bar{Z}^{-1}\bar{\tau}_{rep}. \tag{17a}$$

The stress relaxation time, when "breathing" is able to relax the entire wormlike micelle before reptation can, is given by

$$\tau \sim \bar{\tau}_{rep}\bar{Z}^{-0.5}\varsigma^{0.5}, \quad \varsigma \leq \bar{Z}^{-3}. \tag{17b}$$

An intermediate regime between breathing-dominated and reptation-dominated relaxation occurs when ς is comparable to $\bar{Z}^{-1}$

$$\tau \sim \bar{\tau}_{rep}\bar{Z}^{0.25}\varsigma^{0.75}, \quad \bar{Z}^{-3} \leq \varsigma \leq \bar{Z}^{-1}. \tag{17c}$$

To sum up, stress relaxation times under different conditions are given below

$$\begin{cases} \tau \sim \bar{\tau}_{rep}, & \varsigma \geq 1 \\ \tau \sim \bar{\tau}_{rep}\varsigma^{0.5}, & \bar{Z}^{-1} \leq \varsigma \leq 1 \\ \tau \sim \bar{\tau}_{rep}\bar{Z}^{0.25}\varsigma^{0.75}, & \bar{Z}^{-3} \leq \varsigma \leq \bar{Z}^{-1} \\ \tau \sim \bar{\tau}_{rep}\bar{Z}^{-0.5}\varsigma^{0.5}, & \varsigma \leq \bar{Z}^{-3}. \end{cases}$$

Note that the above formulas can be found in Cates (1987) except that we have replaced α by its equivalent, $\bar{Z}^{-1}$.

By incorporating breathing along with high-frequency Rouse modes [Granek and Cates (1992); Granek (1994)], the deviation from a perfect semicircle at high frequency can be used to estimate the ratio of micelle entanglement length (l_e) to average length ($\langle L \rangle$)

$$\frac{G''_{min}}{G_N} = \left(\frac{l_e}{\langle L \rangle}\right)^{0.8} = \bar{Z}^{-0.8}. \tag{18}$$

Here, G_N is the plateau modulus and G''_{min} is the local minimum of G'' in the Cole-Cole plot at high frequency. Note that for micelle solutions with $\bar{Z}^{-3} \leq \varsigma \leq \bar{Z}^{-1}$, as ς decreases, the minimum gets shallower [Cates (1987); Granek and Cates (1992); Granek (1994)] until ς becomes comparable to $\bar{Z}^{-3}$, which only occurs for micelles with a large number of entanglements ($\bar{Z}$).

Besides adding high frequency relaxation dynamics into the original model, Granek and Cates (1992) also developed a simulation method based on the "Poisson renewal process." By neglecting correlations of micelle length between breakage/rejoining events and assuming that micelle lengths follow a Poisson distribution [Eq. (15)], the relaxation modulus $G(t)$ for wormlike micellar solutions can be described by extending Eq. (13) to polydisperse lengths. Using numerical simulations, the following stress relaxation time was obtained [Granek and Cates (1992)]:

$$\tau = 0.69\bar{\tau}_{rep}(\varsigma^{1/2} + C\varsigma^{2/3}) \ , \tag{19}$$

where C is a correction coefficient accounting for effect of high frequency relaxation dynamics.

C. Experimental measurements and limitation of Cates' model

Experimental characterization of micelle structure has significantly contributed to the development of the theory of wormlike micelle dynamics. The value of the persistence length was measured by Porte *et al.* (1980), who showed that elongated micelles should be thought of as semi-flexible polymerlike chains, rather than as rods. Since then, many important measurement methods have been applied to micellar solutions: SANS (small angle neutron scattering) [Marignan *et al.* (1989); Appell and Marignan (1991)], birefringence [Shikata *et al.* (1994); Decruppe and Lerouge (1999)], DLS/SLS (dynamic/static light scattering) [Brown *et al.* (1989); Nemoto *et al.* (1995)], cryo-TEM (cryogenic transmission electron microscopy) [Clausen *et al.* (1992)], NSE (neutron spin echo) [Nettesheim and Wagner (2007)], and DWS (diffusing wave scattering) [Galvan-Miyoshi *et al.* (2008)]. Table I shows that the measured persistence lengths are typically in the range 20–50 nm, and the micelle diameter is approximately 4 nm.

Although these measurements supply inputs to Cates' model, its predictive ability is limited by some shortcomings.

(1) The average micelle length is not readily obtained from the above methods, and the value extracted from rheological data using Cates' model is usually a fraction of a micron, which is shorter than one would expect based on the rather high value of micelle scission energy [Larson (2012)]. (2) The model does not account for the effects of the persistence length (l_p) nor allow it to be estimated from rheological properties [Oelschlaeger *et al.* (2010)]. (3) The accuracy of rheological predictions is questionable for solutions in the crossover region between "loose" and "tight" entanglements, as discussed below. (4) The treatment of high frequency relaxation mechanisms is oversimplified and lacks consideration of micelle bending modes. (5) The correlation of

TABLE I. Experimental values of l_p and $d/2$ from the literature.

Literature	Method	System	l_p (nm)	$d/2$ (nm)
Marignan *et al.* (1989)	SANS	CPyBr/NaBr	—	1.85–2.4
Appell and Marignan (1991)	SANS	$CPyClO_3$/NaBr	17 ± 5	2 ± 0.1
Gamez-Corrales *et al.* (1999)	SANS	CTAT/NaCl	38 ± 2	2.1 ± 0.05
Magid *et al.* (2000)	SANS	CTA26ClBz + CTAC/Na26ClBz + NaCl	17–34	1.76–2.25
Croce *et al.* (2003)	SANS	EHAC/KCl	—	2.1
Schubert *et al.* (2003)	SANS	CTAT + SDBS/NaTosylate	20–85	2.12–2.16
Kuperkar *et al.* (2008)	SANS	CTAB/$NaNO_3$	—	2.28
Porte *et al.* (1980)	Birefringence	CPyBr/NaBr	20	3
Shikata *et al.* (1994)	Birefringence	CTAB/NaSal	26	—
Appell *et al.* (1982)	SLS	CPyBr/NaBr	20 ± 5	—
Imae *et al.* (1986)	SLS	CTAB/NaBr	42–53	2.3
Brown *et al.* (1989)	DLS	CTAB/Naphthalenesulfonate	36	—
Imae (1990)	DLS	C_{16}TASal/NaSal	111–142	—
Nettesheim *et al.* (2007)	NSE	CTAB/NaSal	24	—
Willenbacher *et al.* (2007)	DWS	CPyCl/NaSal	31–34	—
Galvan-Miyoshi *et al.* (2008)	DWS	CTAB/NaSal	29–45	—
Oelschlaeger *et al.* (2009)	DWS	CPyCl/NaSal	26–30	—
Oelschlaeger *et al.* (2010)	DWS	CTAB/KBr, CTAB/$NaNO_3$, CTAB/$NaClO_3$	40, 34, 29	—

micelle length after a breakage/rejoining with that before such an event is neglected. (6) CR or tube rearrangement is neglected.

Thus, an improved theory is desirable. In what follows, we present a more detailed description of micelle relaxation processes and a simulation method that accounts for these details.

D. Relaxation theory

1. CLFs

CLFs are Rouse-like fluctuations that allow the chain to wrinkle and unwrinkle in its tube, vacating ends of the tube, and relaxing stress [Dealy and Larson (2005)]. CLFs lead to a shortening of reptation time (τ_{rep}^{F}), as estimated by Doi and Edwards (1986)

$$\tau_{rep}^{F} \approx \tau_{rep}^{NF}\left(1 - \frac{1.47}{\sqrt{Z}}\right)^2. \tag{20}$$

In the above, the superscript "*NF*" denotes the pure reptation, while "*F*" denotes the CLF-affected reptation. We note here that a more accurate expression [Eq. (21)] was derived by Likhtman and McLeish (2002)

$$\frac{\tau_{rep}^{F}}{\tau_{rep}^{NF}} = 1 - \frac{2C_1}{\sqrt{Z}} + \frac{C_2}{Z} + \frac{C_3}{Z^{1.5}}, \tag{21}$$

where $C_1 = 1.69, C_2 = 4.17, C_3 = -1.55$.

Beyond this simple correction of the reptation time, Milner and McLeish (1998) developed a mathematical expression that accounts for the time-dependent relaxation

produced by CLFs. By treating a linear chain as a two-armed star with fixed center, they obtained the following relationship for the shrinkage of the unrelaxed tube as a function of time:

$$\langle l_t^2 \rangle = \frac{4N_K b_K^2}{3\pi^{1.5}} \left(\frac{t}{\tau_R} \right)^{0.5}. \tag{22}$$

Here, l_t is the lost tube length at each end through fluctuations, and the brackets $\langle \cdot \rangle$ denote an ensemble average. However, this formula leaves out the shrinkage of tube due to reptation, which becomes ever more important as relaxation progresses. To include contributions from both reptation and CLFs, we first take a time derivative of both sides of Eq. (22), and then use Eq. (22) to replace time t on the right side with $\langle l_t^2 \rangle$, giving

$$\frac{d\langle l_t^2 \rangle}{dt} = \frac{8 b_K^2 k_B T}{3\pi \zeta_K \langle l_t^2 \rangle}, \tag{23}$$

where the definition of Rouse time (τ_R) [Eq. (7)] has been used in deriving the above equation. Substituting Eqs. (1), (5), and (12) into Eq. (23) yields

$$\frac{d\langle l_t^2 \rangle}{dt} = \frac{16 D_0 l_p}{3\pi \langle l_t^2 \rangle}. \tag{24}$$

The advantage of Eq. (24) over Eq. (22) is that the former does not contain time t explicitly as Eq. (22) does but instead describes the rate of loss of occupied tube due to CLFs. This allows us to add this rate to the rate of loss of tube length through reptation, as we describe later.

2. CR

In addition to the above mechanisms, chain relaxation can also occur due to motion of the surrounding chains, i.e., due to CR. Because of its complexity, no general, rigorous theory has been developed for CR, especially for micelles or "living polymers" with breakage and rejoining kinetics. However, a simple model of CR, called double reptation [Tuminello (1986); des Cloizeaux (1988); Tsenoglou (1991)], has been found to capture much of its effect in ordinary polymers, especially when the length distribution is polydisperse, which is always the case for micellar solutions. Double reptation gives the following simple formula [Dealy and Larson (2005)] for CR effect on relaxation modulus [$G(t)$]:

$$G(t) = G_N \mu^2(t), \tag{25}$$

where $\mu(t)$ is the stress relaxation function or the probability for a single chain to relax in a fixed entanglement matrix, i.e., in the absence of CR. Thus, as a simple but effective treatment of CR effects, double reptation is incorporated in our method.

3. Rouse modes

For entangled solutions, long-range Rouse motions for monomers are impeded by topological constraints; the contribution of Rouse motions is thereby confined to a distance of order l_e along the chain. At such short length scales, its contribution is only significant

at high frequencies. These high-frequency Rouse motions result in the following contributions to G' and G'' [Wang *et al*. (2010)]:

$$G'(\omega) = G_N \frac{5(\omega\tau_e)^2}{4} \sum_i \frac{\phi_i}{Z_i} \sum_{p=Z_i}^{N_e Z_i} \frac{1}{(\omega\tau_e)^2 + 4(p/Z_i)^4}, \tag{26a}$$

$$G''(\omega) = G_N \frac{5\omega\tau_e}{4} \sum_i \frac{\phi_i}{Z_i} \sum_{p=Z_i}^{N_e Z_i} \frac{2(p/Z_i)^2}{(\omega\tau_e)^2 + 4(p/Z_i)^4}, \tag{26b}$$

where ϕ_i is the volume fraction of micelles with length L_i; ω is the frequency; N_e is the number of Kuhn steps in a single tube segment (l_e/b_K), which is here made an integer by rounding down, and τ_e is the equilibration time. In the above, p is the mode number of the Rouse motions. Note that the lowest mode number for each chain is equal to the number of entanglements Z_i in the chain, since we are only accounting for Rouse motions localized to within a tube segment, as discussed in reference [Wang *et al*. (2010)]. In both Eqs. (26a) and (26b), the outer sum is a sum over a discrete distribution of micelle species indexed by "*i*."

The volume fraction (ϕ_i) of micelles with length L_i can be expressed in terms of the number density [$N(L_i)$], where this number density distribution is now taken to be discrete, summing to unity

$$\phi_i = N(L_i) L_i \frac{\pi d^2}{4}. \tag{27}$$

4. Semi-flexibility and bending modes

a. Entanglement regimes and semi-flexibility. For entangled chains, two different scenarios are depicted in Fig. 1 depending on the flexibility: Case (a) occurs when the chain can form a random-walk coil within a single tube segment of length a, while for case (b), it can only bend slightly over this distance. The above two scenarios are called loosely and tightly entangled, respectively. Cates assumed that micellar solutions lie in the loosely entangled regime, which we are now finding to be inaccurate for some micellar solutions [Galvan-Miyoshi *et al*. (2008); Oelschlaeger *et al*. (2009); Oelschlaeher *et al*. (2010)].

Therefore, in this paper, both loosely and tightly entanglements are handled more carefully by introducing the parameter (α_e), which is the ratio of entanglement length to persistence length, as given by Eq. (9). Thus, in the loosely entangled regime ($\alpha_e > 2$),

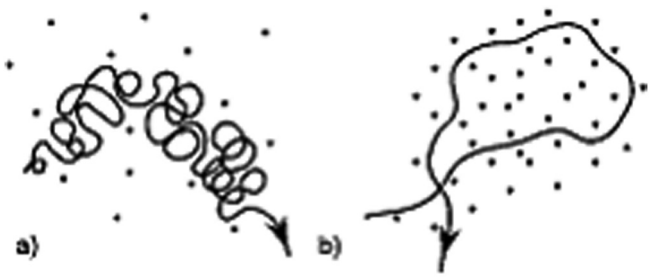

FIG. 1. Loose and tight entanglement regimes [Reprinted with permission from Morse (1998a). Copyright 1998 American Chemical Society].

the tube diameter (a) is larger than the Kuhn length (b_K). For the tightly entangled regime ($\alpha_e < 1$), a is less than the persistence length (l_p). And we take the crossover between these regimes to occur within the range $1 \leq \alpha_e \leq 2$. By applying Eqs. (10) and (11), the relationships between the micelle length (L) and its corresponding tube length (L_t) for these regimes are

$$L_t \approx L, \quad \alpha_e < 2, \tag{28a}$$

$$L_t \approx L/\sqrt{0.5\alpha_e}, \quad \alpha_e > 2. \tag{28b}$$

Thus, in both the tight entanglement and crossover regimes ($\alpha_e < 2$), the tube length is approximately equal to the micelle length.

Although the plateau modulus (G_N) is often determined empirically by doubling the value of measured modulus at the crossover of G' and G'' [Couillet *et al*. (2004)], it can also be calculated theoretically. In the loosely entangled regime, G_N can be derived from blob theory [Khatory *et al*. (1993); Heo *et al*. (2005)]

$$G_N = A\frac{k_BT}{\xi^3}, \tag{29}$$

where ξ is the mesh size [See Eq. (3)]. Here, we introduce a prefactor A which is absent from the original equation in Cates' paper [Turner and Cates (1991)]. The theoretical derivation of its value $A = 9.75$ from established correlations for loosely entangled polymers is given in Appendix A.

On the other hand, in the tight entanglement regime G_N is given by [Morse (1998b)]

$$G_N = \frac{7}{5}\frac{\rho k_BT}{l_e}, \tag{30}$$

where, as defined earlier, ρ is the micelle contour length per unit volume, which is related to micelle diameter (d) and surfactant volume fraction (ϕ) by

$$\rho = \frac{4\phi}{\pi d^2}. \tag{31}$$

Since in many cases, micellar solutions lie between the tight and loose entanglement regimes, we here present a crossover formula to obtain the plateau modulus for any ratio (α_e) of entanglement length to persistence length, namely,

$$G_N = f(\alpha_e)\cdot 9.75\frac{k_BT}{\alpha_e^{9/5}l_p^3} + [1-f(\alpha_e)]\cdot\frac{28}{5\pi}\frac{\phi k_BT}{d^2\alpha_e l_p}. \tag{32a}$$

In the above, we take the weight function $f(\alpha_e)$ to be

$$f(\alpha_e) = \frac{\alpha_e^n}{n+\alpha_e^n}, \tag{32b}$$

where the value n sets the steepness of the cross-over between the formulas for loose and tight entanglements [Eqs. (29) and (30)] Here, we set $n = 3$ to give a relatively rapid, but smooth, crossover, as shown in Fig. 2. We note that at higher concentrations where one enters the tight entanglement regime, one might not expect the blob theory to be

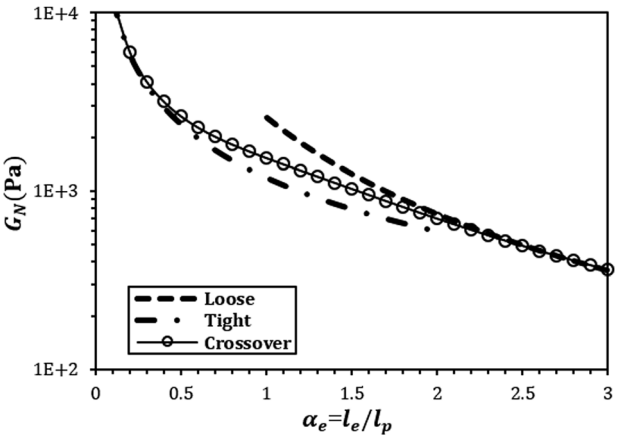

FIG. 2. Plateau modulus for loose and tight entanglement regimes and the crossover between them (for $T = 300\,\mathrm{K}$, $l_p = 25\,\mathrm{nm}$, and $d = 5\,\mathrm{nm}$).

applicable. But the crossover formula, Eq. (32a), is designed to transition away from the prediction of the blob theory [Eq. (29)] to that for tight entanglements [Eq. (30)] as the entanglements become tight, so the failings of the blob theory at high concentration should have negligible impact.

b. Bending modes. The relaxation dynamics introduced in parts 1 through 3 involve length scales larger than persistence length (l_p) for which chains are flexible and high frequency relaxation dynamics is governed by Rouse modes. However, on length scales smaller than l_p, chain segments are effectively elastic rods [Morse (1998a)], whose dynamics are governed by bending motions whose elastic modulus $B(\omega)$ [Morse (1998b); Pasquali *et al.* (2001)] was given by Morse and Macintosh [Morse (1998b); Gittes and MacKintosh (1998)]

$$B(\omega) = \frac{2^{3/4} k_B T}{l_p} \left(i\omega\tau_p\right)^{3/4}, \quad \tau_p = \frac{\zeta_\perp l_p^3}{k_B T}, \tag{33a}$$

where $\zeta_\perp$ is drag coefficient for perpendicular bending motion, given by Batchelor as [Batchelor (1971); Morse (1998b)]

$$\zeta_\perp = \frac{4\pi\eta_s}{\ln(0.6\xi/d)}. \tag{33b}$$

Due to the short length scales over which it contributes to the modulus, bending is only important at frequencies ($\omega > 1/\tau_p$) higher than those for flexible Rouse motions. Thus, contributions to the storage and loss modulus from bending motions are

$$G'(\omega) = Re\left[\frac{B(\omega)\cdot\rho}{15}\right], \quad G''(\omega) = Im\left[\frac{B(\omega)\cdot\rho}{15}\right] + \omega\eta_s, \tag{34}$$

where the definition of ρ is given by Eq. (31). Equations (33) and (34) yield a three-quarter power law for G'' at high frequency, which has been confirmed experimentally by both Oelschlaeger's and Galvan's groups [Galvan-Miyoshi *et al.* (2008); Oelschlaeger *et al.* (2009); Oelschlaeger *et al.* (2010)].

E. Functional form of the modulus

The aim of our simulation method described in Sec. IV is to predict linear viscoelasticity from micelle parameters, and, inversely, to devise a method to determine those parameters from rheological data. The latter methodology is valuable because some parameters are difficult to obtain from nonrheological measurements [Appell *et al.* (1982); Imae and Ikeda (1986); Brown *et al.* (1989); Imae (1990); Clausen *et al.* (1992); Shikata *et al.* (1994); Nemoto *et al.* (1995); Magid *et al.* (2000); Schubert *et al.* (2003); Croce *et al.* (2003); Nettesheim and Wagner (2007); Willenbacher *et al.* (2007); Galvan-Miyoshi *et al.* (2008); Oelschlaeger *et al.* (2010)]. Based on the relaxation mechanisms introduced above, the rheology of wormlike micellar solutions is controlled by five *independent* micelle parameters which can be taken to be plateau modulus (G_N), dimensionless breakage rate (ς), average micelle length ($\langle L\rangle$), semi-flexibility coefficient (α_e), and micelle diameter (d). Detailed information about them and how other parameters, such as time scales, are derived from them, can be found in previous parts. Thus, with the above five *independent* parameters, the functional form of the complex modulus G^* can be expressed as

$$G^*(\omega) = \mathcal{F}\left[G_N\mu^2(t,\varsigma,\langle L\rangle,\alpha_e,d)\right] + G^H(\omega). \tag{35}$$

Here, the real and imaginary parts of $G^*(\omega)$ are the storage (G') and loss (G'') moduli, respectively. The dimensionless stress relaxation function μ (fraction of unrelaxed tube segments in the absence of CR) is squared to allow for CR according to the "double reptation" *Ansatz* [Eq. (25)]. $G^H(\omega)$ accounts for contributions from high frequency Rouse and bending modes [Eqs. (26) and (34)] and also depends on the five parameters listed above. In practice, we only add these high frequency modes after we have Fourier transformed [denoted by operation $\mathcal{F}[\cdot]$ in Eq. (35)] the time-dependent function into the frequency-dependent one. Note that the effect of experimental conditions (temperature T, surfactant volume fraction ϕ, and solvent or water viscosity η_s) are implicitly included among the model parameters, although we do not count them among the five parameters listed above.

For use in what follows, we define in Table II a set of "standard" values of parameters to be used in example simulations.

IV. MODELING

A. Polydispersity

In thermal equilibrium, wormlike micelles are polydisperse in length. Two simple approaches, i.e., (i) mean-field theory (MFT) and (ii) scaling theory, give relationships between average micelle length ($\langle L\rangle$) and scission free energy (E) [Cates (1988); Candau *et al.* (1989); Cates and Candau (1990)]

TABLE II. Standard values of parameters.

	Experimental conditions			Model parameters				
Section	T (K)	ϕ	η_s (cP)	l_p (nm)	ς	$\langle L\rangle$ (nm)	α_e	d (nm)
IV C	300	0.1	0.891	15	0.005	80 l_p	3	3
VI	300	0.1	0.891	25	0.05	80 l_p	2	5

Note: Persistence length (l_p) can be used to obtain the plateau modulus (G_N) once other micelle parameters (ς, $\langle L\rangle$, α_e, and d) as well as temperature T and surfactant volume fraction ϕ are known [see Eq. (32)].

$$\langle L\rangle_{MFT} \sim \phi^{0.5}\exp(E/2k_BT), \tag{36a}$$

$$\langle L\rangle_{scaling} \sim \phi^{0.6}\exp(E/2k_BT). \tag{36b}$$

The scaling result differs from that for MFT because of its inclusion of the excluded volume repulsion. Unfortunately, the above two equations cannot readily be used to extract average micelle length, since E is hard to determine from experiments. For this reason, the average micelle length is usually obtained by fitting of rheological data.

In our simulation method, the exponential micelle length distribution [see Eq. (15)] is discretized into segments with segment length $\Delta L \sim O(l_p)$. The discretized distribution function relates the micelle length ($m_i\Delta L$, with m_i the number of segments in the micelle) to the corresponding number n_i of micelles with this length

$$n_i = Int[num\cdot\exp(-m_i/M)]. \tag{37}$$

Here, "*Int*" is the integer function which rounds the argument down to nearest integer, *num* ($num = 10\,000$) is the total number of micelles in the simulation ensemble; M is the number of segments for a micelle with average length, so that m_i varies from 1 to several times M. Note n_i, M, m_i, i are all integers in our simulation method, with the value of m_i determined by minimizing the error between continuous and discrete micelle length distributions.

B. Pointer algorithm

1. Motivation

Since breakage/rejoining of micelles accelerates relaxation by creating new unrelaxed micelle ends, an appropriate treatment of micellar breakage/rejoining is the key element for any model of wormlike micellar solutions. In 1987, Cates developed a particle diffusing method coupled with random end-hop processes to describe breakage/rejoining of micelles (see Fig. 3). His method is efficient, if only the curvilinear diffusivity (reptation) is included. Further improvements are attained by adding other relaxation dynamics (CLF and Rouse motion). A more sophisticated method was developed by Granek and Cates (1992) in their Poisson renewal process, where a survival time for individual micelles is introduced to describe the occurrence of breakage/rejoining events. However, their model does not account for chain length correlations across breakage/rejoining events nor does it include CR or the crossover to tight entanglements. Thus, improvements are still required.

2. Pointer algorithm

Here, we account for both the living feature of micelles and their polymerlike relaxation mechanisms using a large ensemble of around 10 000 wormlike micelles. Rather than dealing with all Kuhn segments in these chains, it is more efficient to track only the locations of pointers that separate the unrelaxed from the relaxed segments along a discretized micelle, as illustrated in Fig. 4. Then, by summing the fraction of unrelaxed segments between the pointers for all micelles, the linear stress relaxation function (μ) in the absence of CR can be calculated.

3. Breakage and rejoining with pointer algorithm

With the above pointer algorithm, the breakage and rejoining of micelles can be described as creations and annihilations of pointers. When two micelles fuse as shown in

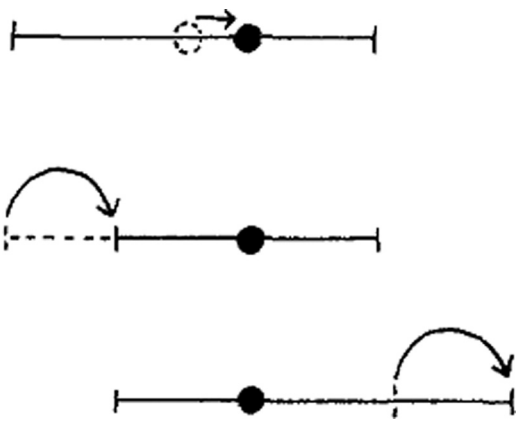

FIG. 3. Diffusing method with end-hop process [Reprinted with permission from Cates, M. E., "Reptation of living polymers: Dynamics of entangled polymers in the presence of reversible chain-scission reactions," Macromolecules **20**, 2289–2296 (1987). Copyright 1987 American Chemical Society].

Fig. 5(a), pointers do not disappear but are retained within the fused micelle to indicate the unrelaxed portions of the new, longer micelle. For micellar breakage [see Fig. 5(b)], a new pair of pointers is added, one at each new end created by the breakage. As the simulation proceeds, the number of pointers can increase, but eventually decreases due to the pointer annihilation process: When two pointers meet each other, both are removed, because the portion of the chain between them is completely relaxed. Since short chains relax very rapidly, the total number of pointers in the simulation is not enormous; it is comparable to the number of micelle ends ($\sim$10 000), which is much smaller than the total number of Kuhn segments ($\sim$1 000 000) in the micelle ensemble.

The detailed simulation procedure for breakage and rejoining can be found in Fig. 6, where the total number of micelles in the ensemble is allowed to fluctuate. During each time step, every segment is given an equal probability to break. Thus, longer chains are more likely to break. Since rejoining is independent of micelle length, any two chain ends have an equal probability to fuse. To maintain upper and lower bounds on the exponential length distribution during the simulation, the shortest micelles (one-segment chains) are not allowed to break, while the longest micelle is not allowed to fuse with any other micelles. And also no new micelle formed by rejoining is allowed to have length greater than the longest one allowed. The above criterion is sensible since the longest chain breaks very quickly and so is not able to retain its length for very long. Since two sequential breakage/rejoining events cannot be allowed to occur within one time step, the

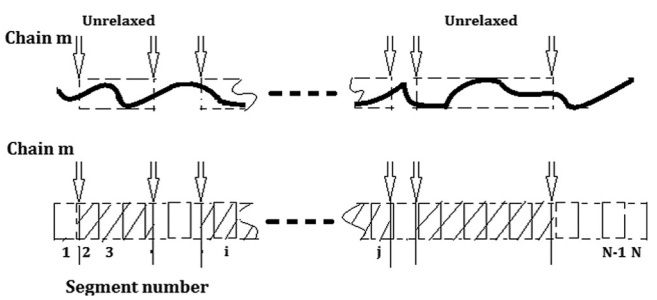

FIG. 4. Pointers along discretized micelles. The shaded segments are the unrelaxed ones.

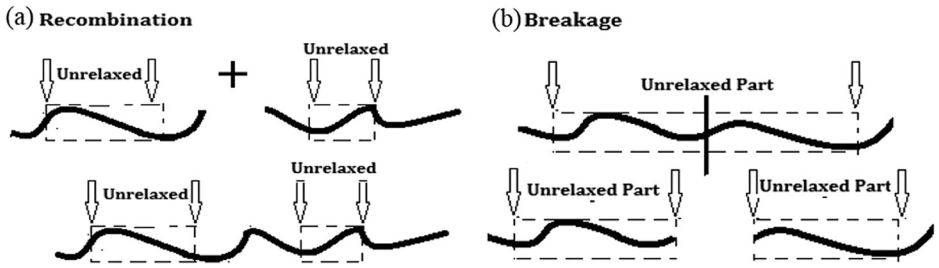

FIG. 5. Breakage and rejoining depicted by pointer algorithm: (a) Rejoining, (b) breakage.

simulation time step should not be larger than the average time required for one micelle in the whole ensemble to break/rejoin, which is

$$\Delta t \leq \frac{\bar{\tau}_{br}}{2 \cdot num} = \frac{\varsigma \bar{\tau}_{rep}}{2 \cdot num}, \tag{38}$$

where $num = 10\,000$ is the total number of micelles in our simulation ensemble.

The above breakage mechanism is the reversible scission scheme assumed in Cates' original model, as described in Sec. III B. However, additional "end-interchange" and "bond-interchange" schemes were suggested later by Turner and Cates (1992), which involve "three-arm" and "four-arm" intermediates. Although we do not consider these schemes in this paper, the pointer algorithm can readily be modified to include them as we hope to discuss in a future paper.

4. Relaxation with the pointer algorithm

With a pointer on each end of each micelle, the relaxation process induced by reptation is equivalent to the random movement of both two pointers on a micelle in the same direction and by the same amount, whose direction is uncorrelated from one time step to the next [see Fig. 7(a)]. The distance (Δl_R) of such a movement in a single time step is given by

$$\Delta l_R = \sqrt{2D_c \Delta t}. \tag{39}$$

Since the effect of CLF is significant at early times, we include its contribution by adding additional movement (Δl_F) of the pointers [see Fig. 7(b)]. However, Eq. (22) cannot be used throughout the simulation because it contains an explicit dependence on time t and is not valid when reptation and breakage/rejoining are also occurring. Thus, we normally use Eq. (24) and deploy Eq. (22) only when Eq. (24) breaks down because a pointer reaches the end of a micelle. That is, we use

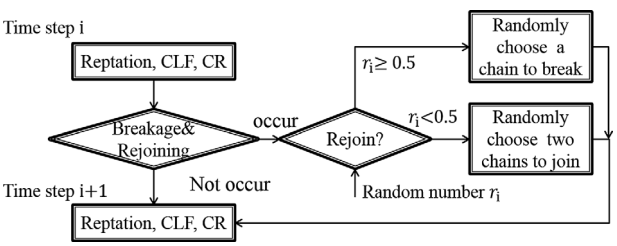

FIG. 6. Procedure for multiple breakage/rejoining cycles.

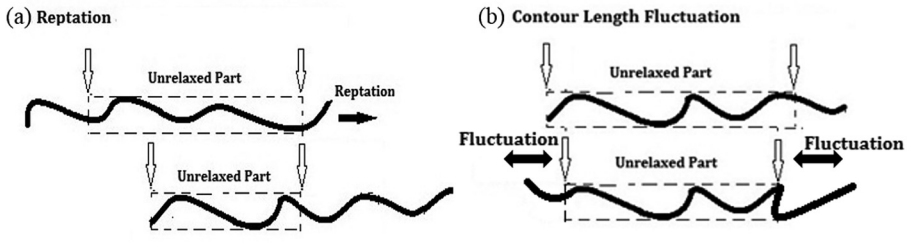

FIG. 7. Reptation and CLF depicted by pointer algorithm: (a) Reptation, (b) CLFs.

$$\Delta l_F^2 = \frac{16 D_0 l_p \Delta t}{3\pi l^2}, \quad l \geq l_p, \tag{40a}$$

$$\Delta l_F^2 = \frac{8 L l_p}{3\pi^{1.5}} \left(\frac{\Delta t}{\tau_R}\right)^{0.5}, \quad l < l_p. \tag{40b}$$

Here, Δl_F is the CLF-induced additional movement of a pointer, whose sign is chosen always to reduce the size of unrelaxed region of the tube; l is the length of the relaxed end of a micelle during the current time step. Note that apart from making l large enough to switch to Eq. (40a), Eq. (40b) acts as the initialization for CLF, which has negligible effect on the overall relaxation process.

To increase the accuracy, we apply an iterative method to Eq. (40a)

$$\Delta l_{F,i+1}^2 = \frac{16 D_0 \Delta t l_p}{3\pi \left(l + \Delta l_{F,i}/2\right)^2}, \quad l \geq \Delta L. \tag{40c}$$

To calculate $\Delta l_{F,i+1}$, five iterations are used, which we found gives nearly converged results that are insensitive to the time step.

5. Other relaxation mechanisms (CR and Rouse and bending relaxation modes)

For CR, double reptation is applied according to Eq. (25). Since a direct simulation of high frequency behavior would require a tiny time step and huge computational cost, we add analytic forms for the Rouse and bending motions [Eq. (26) and Eqs. (33) and (34)] to simulation results after they have been transformed to the frequency domain.

C. GA

To reduce the computational cost for postsimulation processing, the data are recorded in logarithmic time intervals, since the simulation data can span across several decades of time with typically millions of time steps. According to Eq. (38), the upper bound of the time step depends on the dimensionless breakage rate (ς). In addition, early-time (high-frequency) behavior needs to be determined precisely, because for micellar solutions, the high-frequency regime strongly affects the estimates of important microstructural small-length-scale parameters (l_e, l_p, and d), which in turn affect estimates of other parameters. However, the transformation from the time to the frequency domain is a classic ill-posed problem. Here, results (Fig. 8) from two traditional

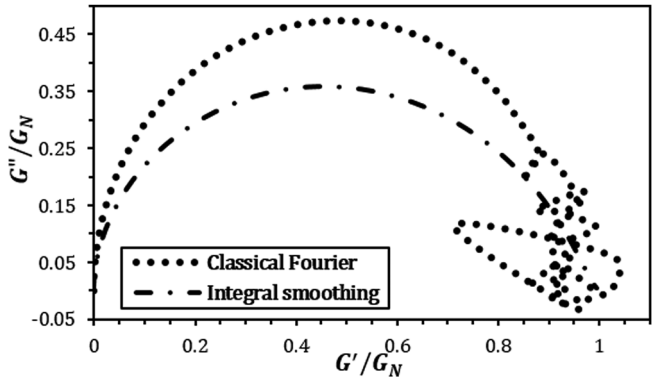

FIG. 8. Results of two traditional transformation methods for the normalized Cole-Cole plot using standard values of parameters.

methods [classical Fourier transform Eq. (41a) and integral smoothing Eq. (41b)] are used to illustrate the difficulties with these transformations. The standard values of parameters used in this section can be found in Table II

$$G'(\omega) = G_N\omega\int_0^T \sin(\omega t)\mu(t)dt, \quad G''(\omega) = G_N\omega\int_0^T \cos(\omega t)\mu(t)dt, \tag{41a}$$

$$G'(\omega) = G_N\int_0^1 \frac{\omega^2 t^2}{1+\omega^2 t^2}\mathrm{d}\mu(t), \quad G''(\omega) = G_N\int_0^1 \frac{\omega t}{1+\omega^2 t^2}\mathrm{d}\mu(t). \tag{41b}$$

As shown by Fig. 8, the classical Fourier transformation gives good results only at low frequencies ($\omega < 500\,\mathrm{rad/s}$) above which large oscillations occur as a result of the ill-posedness of simple integral transform in Eq. (41a). On the other hand, although the integral smoothing method works reasonably well for broad distributions of relaxation times [Dealy and Larson (2005)], the height of the G''/G_N versus G'/G_N curves is underestimated when the distribution of relaxation times is narrow for small ς. This can be seen by comparing the height of the normalized Cole-Cole plot in Fig. 8, where G''/G_N remains below 0.4 for integral smoothing, with that for classical Fourier transformation, where the height exceeds 0.45.

Fortunately, there are standard methods for solving ill-posed problems of the kind faced here. Such methods include Monte Carlo methods, annealing algorithms, and GAs. Here, we choose to develop a GA because of its stability, nonlocality, and insensitivity to initial guess. A more detailed description of our GA is given in Appendix B, which also shows that our GA avoids the problems discussed above.

V. SIMULATION TESTING

We tested that the model gives the correct equilibrium distribution of micelle lengths, captures the relaxation dynamics of pure reptation and with added CLFs correctly, and converges with increasing simulation runs and ensemble size. Testing details are given in Appendix C.

VI. ANALYSIS AND DISCUSSION

We now address the relationships between rheological predictions (G' and G'' curves) and the micelle parameters ($G_N, \varsigma, \langle L \rangle, \alpha_e$, and d). We will describe both the determination of linear rheology from micelle parameters, and, conversely, the extraction of micelle parameters from measured linear rheological properties. Standard values of parameters, given in Table II, are used in this section. Note that the base of following logarithm functions (denoted as "log") is 10.

A. From micelle parameters to rheology

1. Simulation procedure

As described by Eq. (35), five important *independent* parameters ($G_N, \varsigma, \langle L \rangle, \alpha_e$, and d) are necessary to predict the rheology of wormlike micellar solutions over a wide frequency range. With these parameters as inputs, linear rheological behavior is obtained by simulating the time-dependent relaxation of a polydisperse micelle ensemble. A flowchart describing the sequence of calculations, and the flow of inputs and outputs for each calculation, is shown in Fig. 9.

2. Relaxation mechanisms with breakage/rejoining

By running simulations following the procedure depicted in Fig. 9, we can determine the effects of each relaxation mechanism on the rheology. Our simulations show that an increase in the parameter α_e (ratio of micelle entanglement length to persistence length) speeds relaxation for fixed ς and $\langle L \rangle$. The reason is that increase in α_e allows micelles to form coils within individual tube segments, thus reducing tube length ($\langle L_t \rangle$) through Eq. (28), which speeds relaxation.

Since the characteristic time [τ_R, Eq. (7)] for CLFs is typically 1–2 orders of magnitude lower than that for reptation [Eq. (8)], inclusion of CLFs adds short relaxation times to the relaxation process. Thus, a larger deviation from the Maxwell model (monoexponential relaxation or perfect semi-circle in Cole-Cole plot) is expected when CLFs are present than when only pure reptation occurs. Note that the effects of some parameters ($\langle L \rangle$ and α_e) cannot be observed in Cole-Cole plots, for these parameters mainly affect the overall relaxation rate, and the Cole-Cole plot contains no absolute frequency or time information.

As with CLFs, double reptation increases deviations from the Maxwell model, in the latter case by squaring the stress relaxation function. The effect of double reptation can be easily seen in Fig. 10 by lowering height of the Cole-Cole semi-circle. Since fast local motions (Rouse and bending) are not affected by the slower relaxation dynamics discussed thus far, the contributions of Rouse and bending dynamics are simply added to the

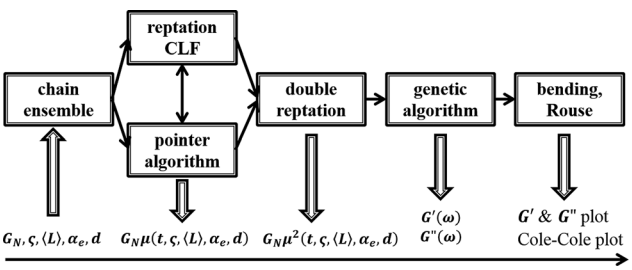

FIG. 9. Flowchart describing steps in the calculation.

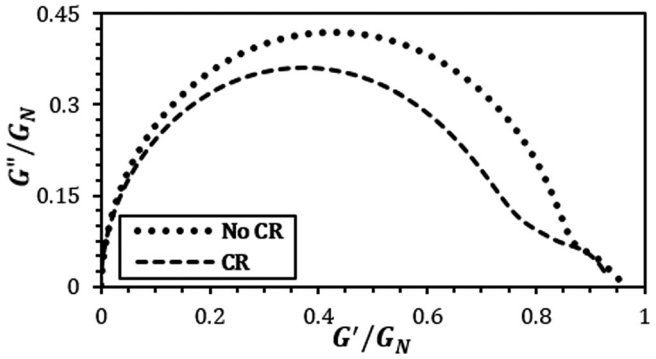

FIG. 10. Effect of double reptation on the normalized Cole-Cole plot.

simulation results analytically. These high-frequency modes produce a "dip" in the Cole-Cole plot where G'' goes through a minimum. Confirmed by simulations with large α_e (for which micelle rigidity is insignificant), a smaller average number of entanglements ($\bar{Z}$) yields a shallower dip and a shift of upturn toward lower frequency, which is leftward on a Cole-Cole plot [Granek (1994)] (Fig. 11). Note that, as shown by Fig. 11, local maxima are also observed at high frequencies ($\omega > 1/\tau_e$) due to the truncation of the high frequency Rouse modes at the frequency at which micelle stiff cuts off these modes [Eq. (26b)]. However, this local maximum disappears when bending modes are added.

3. Scaling laws

Although our method is based on simulations, it is worthwhile to construct approximate scaling expressions for rheological features from the simulations and compare them with those obtained from Cates' model [Cates (1987)] without/with breathing fluctuations (CLFs). A general expression [Eq. (42)] for the stress relaxation time (τ) can be found with prefactor C and power law exponents ($\beta, \gamma,$ and δ) either determined by analytical theory from Cates (1987) and Granek (1994) or from fits to simulation results with parameters varied over experimentally realistic ranges

$$\tau = C\bar{\tau}_{rep}^{\beta}\varsigma^{\gamma}\bar{Z}^{\delta}. \tag{42}$$

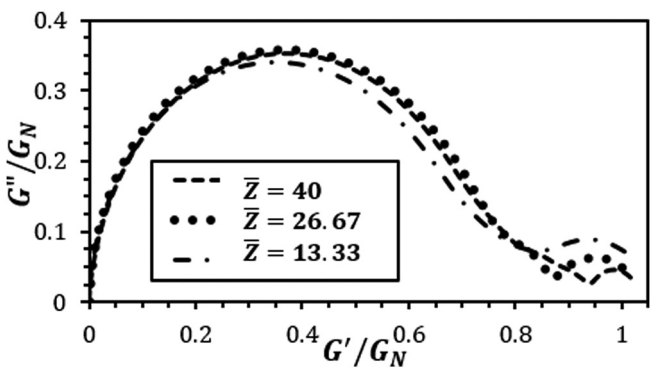

FIG. 11. Dip in the normalized Cole-Cole plot at high frequencies caused by Rouse modes as a function of the number $\bar{Z}$ of entanglements.

TABLE III. Scaling laws for relaxation without CLFs.

Cates' model		Pointer Simulations	
$\tau \sim \bar{\tau}_{rep}$	$\varsigma > 1$	$\tau \sim f(\bar{\tau}_{rep})$	$\varsigma > 200$
$\tau \sim \bar{\tau}_{rep}\varsigma^{0.5}$	$\varsigma < 1$	$\tau \cong 1.50(\bar{\tau}_{rep})^{0.95}\varsigma^{0.56}$	$\varsigma < 10$

Notice that the simulation results can be described by simple power law dependencies on the relevant parameters in the regime: $\varsigma < 10$ (living micelles). For $\varsigma > 200$, micelles are "dead," whose rheological behavior (expressed as a functional dependence) is the same as in a classical polymer solution. Between these two regimes, we do not have a simple scaling formula. It is surprising that the Cates' formula $\tau \sim \bar{\tau}_{rep}\varsigma^{0.5}$ persists to remarkably high values of ς, apparently because the longer micelles in the ensemble are still able to break multiple times before relaxing, and these dominate the terminal relaxation time.

Here, $\tau = 1/\omega_{cross}$, as defined in Sec. II G. Notice that the effect of $\langle L \rangle$ and α_e has been included implicitly in the above equation, since both $\bar{Z}$ and $\bar{\tau}_{rep}$ are functions of $\langle L \rangle$ and α_e. The scaling laws are shown in Tables III and IV for relaxations without/with CLFs, respectively.

After incorporating the high frequency Rouse motions, in early literature, Cates' model has been used to obtain an estimation of the dimensionless average micelle length $\bar{Z} = \langle L \rangle / l_e$ [Eq. (2)] from G''_{min}, the depth of the minimum in G'' relative to the plateau modulus [Eq. (18)]. As described in more detail in Sec. VI B 1 [Eq. (43b), Fig. 17], the corresponding correlation extracted from our simulations is shown here in Table V.

Thus, while the scaling results from our simulations are qualitative similar to those from Cates' model, they are quantitative significantly different.

4. Parameter analysis

In the above, we have assessed the effects of different relaxation mechanisms and parameters on stress relaxation time or on the depth of the minimum in G''. However, their effects on the relaxation curve over the entire frequency region have not yet been considered. Thus, in what follows, we will discuss their effects on the normalized Cole-Cole plot by varying one parameter at a time, leaving others set at their corresponding standard values.

a. Persistence length l_p. We note first that persistence length (l_p) can be used to obtain the plateau modulus (G_N) once other parameters ($\langle L \rangle, \alpha_e, \varsigma, d, T,$ and ϕ) are known. To eliminate the influence of G_N, Cole-Cole plots normalized by G_N are shown in Fig. 12(a) for different values of l_p. According to Eqs. (33) and (34), the value of l_p affects the slope of the "upturn" in G'' after it passes through a minimum and enters the high frequency region, as shown in Fig. 12(a).

TABLE IV. Scaling laws for relaxation with CLFs.

Cates' model		Pointer simulations	
$\tau \sim \bar{\tau}_{rep}$	$\varsigma > 1$	$\tau \sim f(\bar{\tau}_{rep}, \bar{Z})$	$\varsigma > 200$
$\tau \sim \bar{\tau}_{rep}\varsigma^{0.5}$	$\bar{Z}^{-1} < \varsigma < 1$	$\tau \cong 1.39(\bar{\tau}_{rep})^{1.03}\varsigma^{0.62}$	$\bar{Z}^{-1.5} < \varsigma < 10$
$\tau \sim \bar{\tau}_{rep}\varsigma^{0.75}\bar{Z}^{0.25}$	$\bar{Z}^{-3} < \varsigma < \bar{Z}^{-1}$	$\tau \cong 2.11(\bar{\tau}_{rep})^{1.03}\varsigma^{0.74}\bar{Z}^{0.19}$	$\varsigma < \bar{Z}^{-1.5}$
$\tau \sim \bar{\tau}_{rep}\varsigma^{0.5}\bar{Z}^{-0.5}$	$\varsigma < \bar{Z}^{-3}$	—	

Note: Attainment of the fourth Cates regime ($\varsigma < \bar{Z}^{-3}$) requires much smaller values of both ς ($\varsigma \sim 10^{-3}$) and $\bar{Z}$ ($\bar{Z} \sim 10$) than are normally considered and lies outside of the scope of our work here.

TABLE V. Estimations for average micelle length.

Cates' model	Pointer simulations
$\frac{G''_{min}}{G_N} \sim \bar{Z}^{-0.8}$	$\frac{G''_{min}}{G_N} \cong C\bar{Z}_t^{-0.61}, \quad 1 < \alpha_e < 3$

Note: $\bar{Z}$ is greater than or equal to $\bar{Z}_t$ (i.e., the micelle contour length is always equal to or larger than the tube length).

b. Breakage time relative to reptation time ς. Figure 12(b) reveals that as ς decreases, the height of normalized Cole-Cole plot increases and, as expected, the plot becomes more semi-circular, approaching that for a Maxwell model. Thus, the parameter ς has a greater effect than any other parameter on the shape of normalized Cole-Cole plot before the upturn at high frequencies. Note in Fig. 12(b) that as long as ς is less than unity, its effect on the high-frequency upturn is small.

c. Average micelle length $\langle L\rangle$ *and flexibility* α_e. The effects of average micelle length ($\langle L\rangle$) and flexibility coefficient (α_e) on the normalized Cole-Cole plot are similar [see Figs. 12(c) and 12(d)]. (The average micelle length also has a large effect on the terminal relaxation time, but that effect does not show up in a Cole-Cole plot.) Both of them affect the minimum value of G'' while holding the height of semicircle constant. A somewhat flat region around the minimum is also observed when the ratio of $\langle L\rangle$ to l_p exceeds 100 and α_e is no larger than 2. The reason for the flat region for $\alpha_e < 2$ is that micelle stiffness suppresses Rouse modes which would otherwise cause a more gradual change in G'' before the onset of bending modes. Thus, without Rouse modes, a deeper dip is expected and the upturn is postponed to higher frequency.

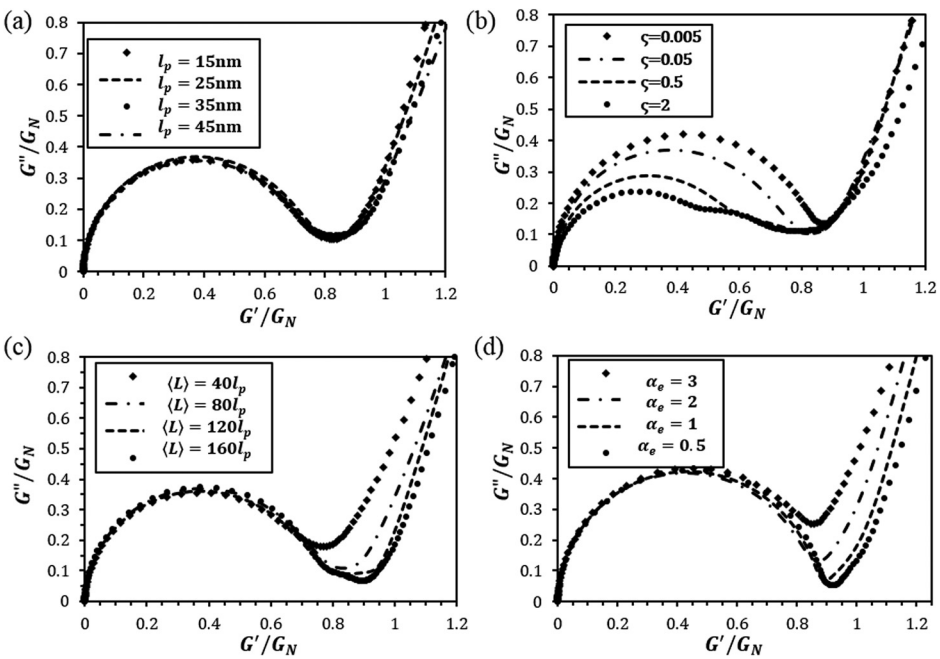

FIG. 12. Effect of model parameters on normalized Cole-Cole plots: (a) l_p, (b) ς, (c) $\langle L\rangle$, (d) α_e.

Thus, a qualitative look at the shape of normalized Cole-Cole plot gives a rough indication of the magnitude of ς and of either $\langle L \rangle$ or α_e. To determine these parameters more precisely, we turn next to development of a systematic method for inferring micelle parameters from rheological behavior.

B. From rheology to micelle parameters

1. Empirical formulas

An iterative simulation procedure to estimate parameters from "global" rheological behavior is developed in this section. Since a proper starting point for further iterations can reduce the total number of iterations and improve the accuracy of final result significantly, we attempt to construct empirical formulas for good initial guesses of parameters through "local" features of rheological curves. Figures 13(a) and 13(b) give the same data but in different formats (frequency and Cole-Cole plot). The points (G'_{max}, G''_{max}) and (G'_{min}, G''_{min}) in Fig. 13(b) correspond to the same points donated as $(\omega_{max}, G'_{max}, G''_{max})$ and $(\omega_{min}, G'_{min}, G''_{min})$ in Fig. 13(a). Note that the subscripts "*max*" and "*min*" represent the maximum and minimum in G''.

a. G_N versus ς. As mentioned above, ς controls the height of the normalized Cole-Cole semicircle, which is negligibly affected by other parameters. A family of curves shown in Appendix D (Fig. 28) obtained by varying ς alone, give heights plotted in Fig. 14. Semi-log fits to the relationships between G''_{max}/G_N versus ς, as well as G'_{max}/G_N versus ς are obtained for ς between 0.001 and 2. As shown in Fig. 14, as ς increases, the difference between G'_{max} and G''_{max} increases, as the Cole-Cole plot deviates more and more from a semi-circle.

b. G_N versus $\bar{Z}_t$. Motived by an equation from Granek (1994) [Eq. (18)] that allows an estimation of L from the ratio G''_{min}/G_N, we now examine the effect of a related quantity, $\bar{Z}_t$ [Eq. (2)], on this dip (G''_{min}/G_N) in a normalized Cole-Cole plot. From the family of curves (Fig. 29 in Appendix D), we have obtained the power-law correlation $(G''_{min}/G_N = C\bar{Z}_t^{-0.61})$ plotted in Fig. 15 with the prefactor C determined approximately in what follows: When $\bar{Z}_t > 30$, the prefactor is set to be unity, and then it increases linearly to 1.5 when $\bar{Z}_t = 10$. The detailed expressions are given in Eq. (43b).

c. $\bar{\tau}_{rep}$ versus ς. Since normalized Cole-Cole plots do not contain either frequency or time, they do not allow estimates of characteristic times such as $\bar{\tau}_{rep}$, which must instead

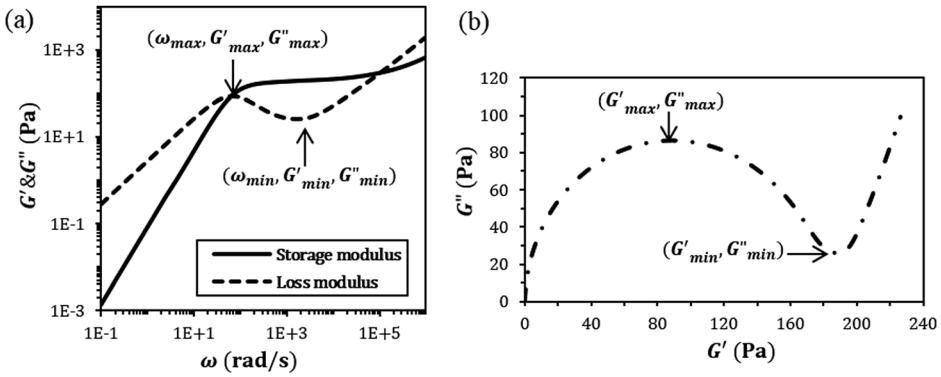

FIG. 13. Definition of significant local rheological features: (a) G' and G'' versus frequency, (b) Cole-Cole plot.

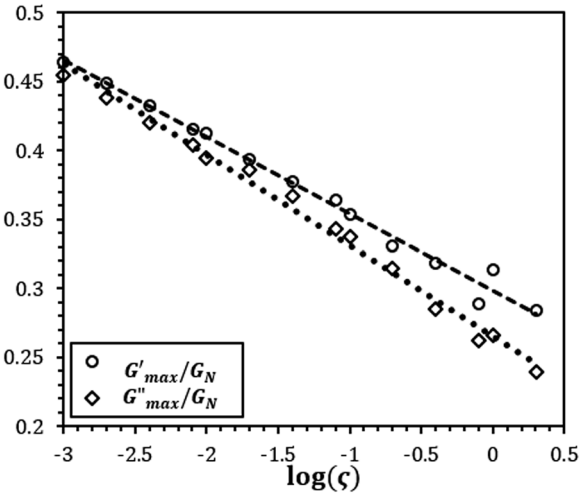

FIG. 14. Empirical correlations for the dependences of G'_{max}/G_N and G''_{max}/G_N on ς with other parameters fixed at standard values. R^2 values of the semi-log fits are as follows: 0.988 for the dashed line; 0.991 for the dotted line.

be obtained from a frequency plot of G'' by constructing an additional equation relating $\bar{\tau}_{rep}$ to the dimensionless breakage rate (ς) and specific frequency (ω_{max}). Our results are shown in Fig. 16, where a power-law formula, with exponent -0.63, for the dependence of $(\omega_{max}\bar{\tau}_{rep})$ on ς and prefactor B is illustrated.

The above results can be summarized by the following empirical formulas:

$$\frac{G'_{max}}{G_N} = -0.0557\log(\varsigma) + 0.298, \quad \frac{G''_{max}}{G_N} = -0.0657\log(\varsigma) + 0.265, \quad \bar{Z} > 10, \quad (43a)$$

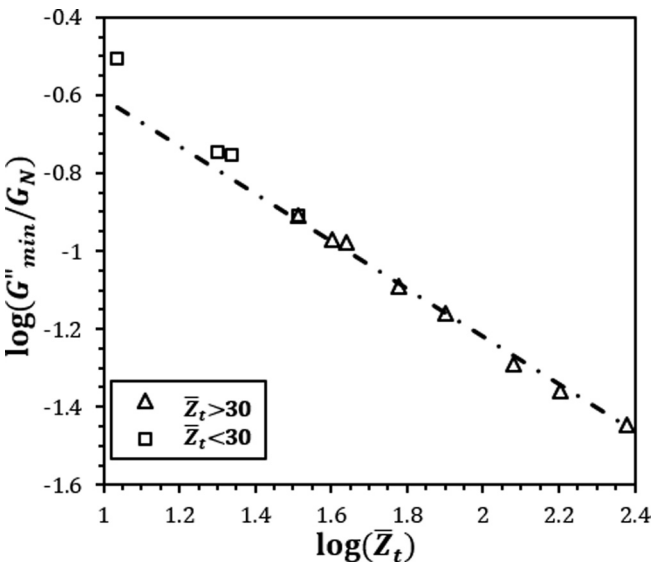

FIG. 15. Empirical correlation for the dependence of G''_{min}/G_N on dimensionless tube length $\bar{Z}_t$ with other parameters fixed at standard values. R^2 value of log-log fit is 0.970.

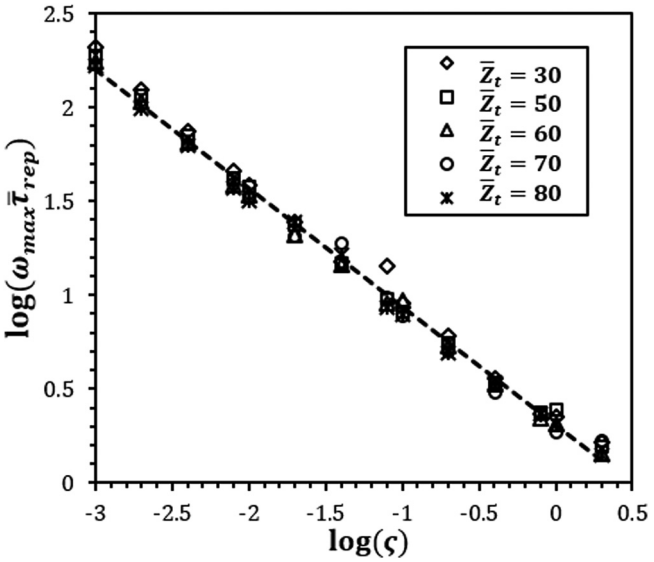

FIG. 16. Empirical correlation for the dependence of $(\omega_{max}\bar{\tau}_{rep})$ on dimensionless breakage rate ς for various values of $\bar{Z}_t$ and other parameters set to standard values. The result can be approximated by Eq. (43c).

$$\frac{G''_{min}}{G_N} = C\bar{Z}_t^{-0.61}, \quad 1 < \alpha_e < 3, \quad \begin{cases} C = 1, & \bar{Z}_t > 30 \\ C = \dfrac{7 - 0.1\bar{Z}_t}{4}, & 30 > \bar{Z}_t > 10, \end{cases} \tag{43b}$$

$$\omega_{max}\bar{\tau}_{rep} = B\varsigma^{-0.63}, \quad B = 2.1 \text{ for } \quad 1 < \alpha_e < 3. \tag{43c}$$

Note that applications of the above correlations are limited to their stipulated regions, outside of which their accuracy cannot be guaranteed. The ranges considered are those needed for comparison to experiments described below. Extension of those correlations to a much wider range of $\bar{Z}$ and α_e will be taken up in future work. However, as one example, we note that the scaling law in Eq. (43b) is invalid in the loose entanglement limit, where α_e is large. However, by replacing $\bar{Z}_t$ with $\bar{Z}$ in Eq. (43b), scaling laws for G''_{max}/G_N versus $\bar{Z}$ valid over a wide range of $\bar{Z}$ and α_e varying from 8 (loosely entangled) to 0.4 (tightly entangled) can be obtained, as shown in Fig. 17.

Now we try to sum up all the equations needed for an initial guess of micelle parameters. For simplicity, detailed expressions for each formula do not appear in this list, and we simply represent the functions by "A", "B", …, "Q"

$$\begin{cases} xG'_{max} + (1-x)G''_{max} = A(G_N, \varsigma) \\ G''_{min} = B(G_N, \bar{Z}_t) \\ \omega_{max} = C(\varsigma, \bar{\tau}_{rep}), \end{cases} \tag{44a}$$

$$\begin{cases} \bar{Z}_t = F(\langle L\rangle, \alpha_e, l_p) \\ \bar{\tau}_{rep} = G(\langle L\rangle, \alpha_e, d, l_p) \\ G_N = H(\alpha_e, d, l_p), \end{cases} \tag{44b}$$

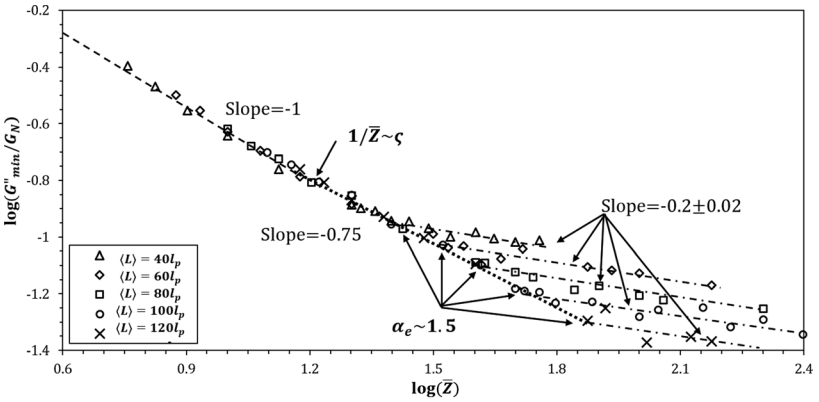

FIG. 17. Extended empirical correlation for the dependence of G''_{min}/G_N on entanglement number $\bar{Z}$ by varying $\langle L\rangle$ and l_e with other parameters fixed at standard values.

$$G^H(\omega) = Q(d, l_p, \omega). \tag{44c}$$

Equation group (44a) comes from empirical formulas in Eq. (43). The three equations in (44b) are derived theoretically by combining Eqs. (2), (9), (28); Eqs. (4), (12), (28); and Eq. (32); respectively, whose detailed expressions are given in Appendix E. The above two groups of equations are used to obtain initial guesses of parameters for the simulation procedure described below. Thus, Eqs. (44a) and (44b) consist of six equations involving 12 parameters including 4 ($\omega_{max}, G'_{max}, G''_{max}, G''_{min}$) that can be extracted simply from rheological curves, and 2 (micelle persistence length l_p and diameter d) that are set to preassigned values initially. This leaves six unknown parameters ($G_N, \varsigma, \langle L\rangle, \alpha_e, \bar{\tau}_{rep}$, and $\bar{Z}_t$) and six equations so that a unique solution is possible. Note that l_p and d can be updated during the simulation based on fitting Eq. (44c) [see Eq. (E4) in Appendix E for detailed expression] to the high-frequency data. If high-frequency data are not available or are not adequate to fit l_p and d unambiguously, then these two parameters must be assigned values from sources other than rheological data, as discussed below. Definitions for all the above parameters can be found in Sec. II.

2. Parameter estimation

Although equation groups [Eqs. (44a) and (44b)] are applied to get the initial guess, these formulas have other uses. By dividing the frequency domain into four different ranges (low, transition 1, transition 2, and high frequency) with three specific frequencies (ω_{max}, ω_{min}, and $10\omega_{min}$), these formulas can tell us which parameters one can estimate by matching specific points or fitting data in each of these frequency ranges. The rheological parameters with their corresponding fitting features and the relaxation mechanisms that dominate in each frequency range are depicted in Fig. 18. An accurate estimate of a parameter can only be achieved by fitting experimental data over a frequency range that contains the rheological features showing the greatest sensitivity to that parameter.

3. Simulation procedure

Based on the analysis in parts 1 and 2, the simulation procedure to extract parameters from rheological behavior is laid out in Fig. 19: Rheological plots (G' and G'' versus

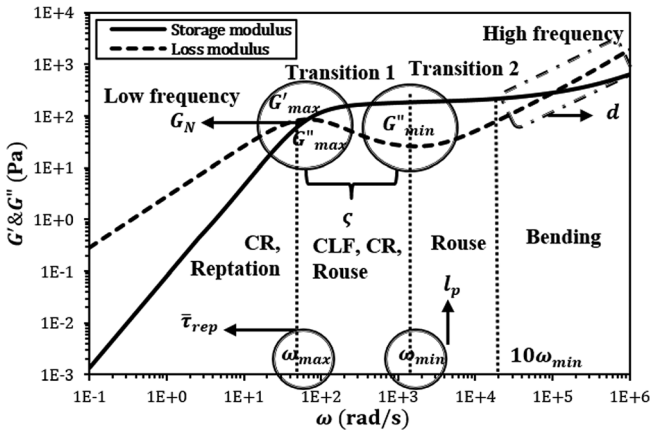

FIG. 18. Dominant relaxation mechanisms and five parameters ($G_N, \varsigma, d, \bar{\tau}_{rep}$, and l_p) controlling the behavior in each of four different frequency ranges. Note that this set of five parameters differs from the set of "five *independent* parameters" described above in that they include $\bar{\tau}_{rep}$ and l_p rather than $\langle L \rangle$ and α_e. However, the set of five parameters extracted from this plot can be converted to our canonical five *independent* parameters using Eq. (44b). One should also note that a system dependent choice of $10\omega_{min}$ as the starting frequency for the bending regime is made here.

frequency) immediately offer us values of $(\omega_{max}, G'_{max}, G''_{max}, G''_{min})$. With the initial guesses of l_p and d as inputs, equations in Eqs. (44a) and (44b) can be solved for six parameters $(G_N, \varsigma, \langle L \rangle, \alpha_e, \bar{\tau}_{rep}$, and $\bar{Z}_t)$. Of these, five *independent* parameters $(G_N, \varsigma, \langle L \rangle, \alpha_e$, and the guessed $d)$ can be used to predict rheological curves based on the procedure in Fig. 9. The difference between simulated curves and the experimental ones $(\Delta G^H, \Delta\omega_{max}, \Delta G'_{max}, \Delta G''_{max}, \Delta\omega_{min}$, and $\Delta G''_{min})$ can then be used as feedback to modify the original guess of these parameters for next iteration. Through optimization, we can get excellent fits with reasonable values of the parameters (shown below). Note that entanglement length (l_e) and persistence length (l_p) are not independent parameters. Their values can be obtained once micelle parameters $(G_N, \varsigma, \langle L \rangle, \alpha_e$, and $d)$ as well as temperature T and surfactant volume fraction ϕ are known. Details of the iteration

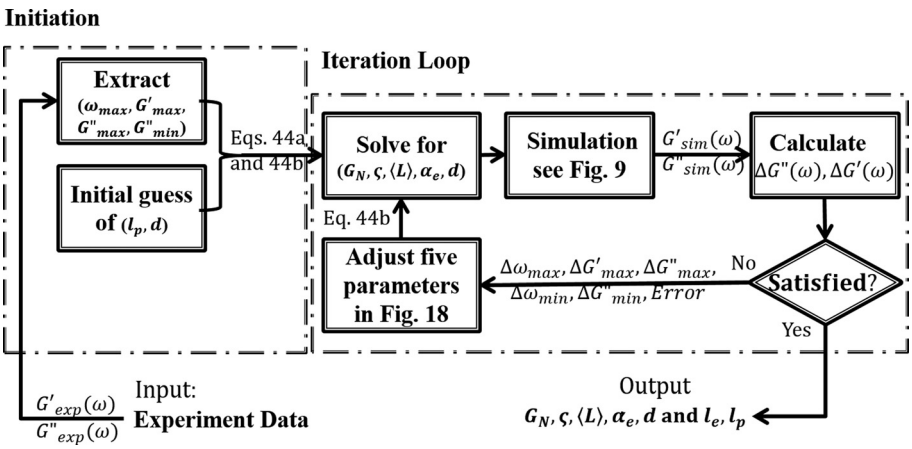

FIG. 19. Schematic of simulation procedure to obtain micelle parameters from rheological behavior.

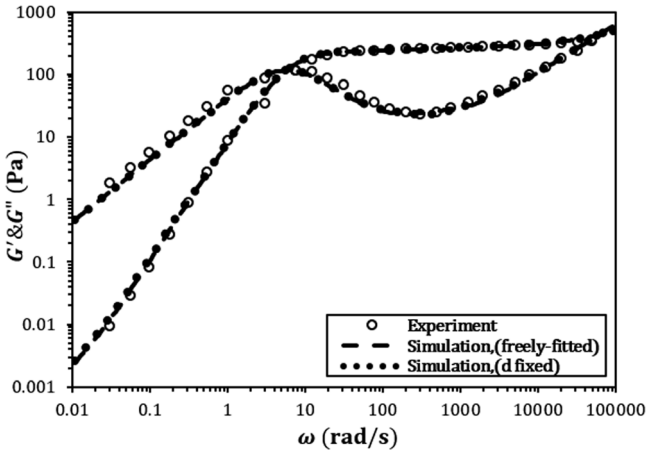

FIG. 20. Simulation results of the Pointer Algorithm fitted to rheological data in Oelschlaeger *et al.* (2010).

procedure and sensitivity of the fits to the parameter values will be addressed in a subsequent paper.

4. Results and discussion

Finally, we present in Figs. 20 and 21 the results of the fitting (with R^2 values of 0.97 and 0.92, respectively, for Figs. 20 and 21) to experimental data ($c_{\mathrm{CTAB}} = 0.35\,\mathrm{mol/L}$, $c_{\mathrm{NaClO3}} = 0.6\,\mathrm{mol/L}, T = 303\,\mathrm{K}$) from Oelschlaeger *et al.* (2010) and ($c_{\mathrm{CTAB}} = 0.15\,\mathrm{mol/L}$, $c_{\mathrm{KBr}} = 1.5\,\mathrm{mol/L}$, $T = 308\,\mathrm{K}$) from Khatory *et al.* (1993). Note that low frequency behaviors ($\omega < 100$ rad/s) were measured by a mechanical rheometer in both cases, while DWS was used by Oelschlaeger *et al.* (2010) to obtain the high frequency data in Fig. 20.

As shown in Figs. 20 and 21, our simulation results successfully match the rheological behavior of micellar solutions in the low and transition frequency ranges. (The deviation at low frequencies in Fig. 21 is likely due to transducer error, since the slope in this region is steeper than the expected terminal slope of 2 for G'.) At high frequencies, an unexpectedly early upturn occurs in the data of Khatory *et al.* (1993) [the upturn

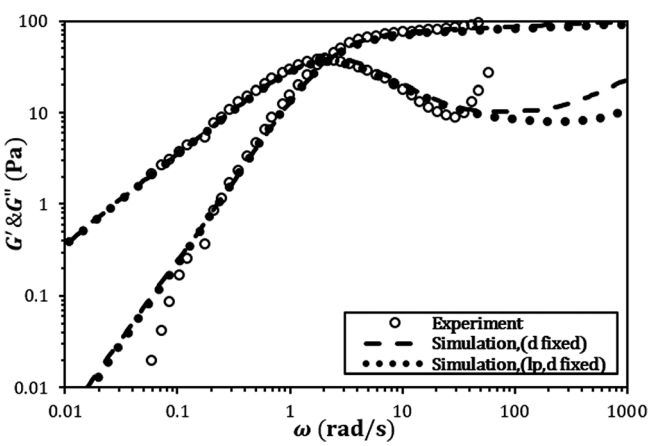

FIG. 21. Simulation results of the Pointer Algorithm fitted to rheological data in Khatory *et al.* (1993).

frequency ω_{min} is ten times smaller than that for Oelschlaeger *et al*. (2010)], which makes our fitting much poorer in this region for the high-frequency mechanical data of Khatory *et al*. than for the high-frequency DWS data in Oelschlaeger *et al*. (2010). The high-frequency data in Khatory *et al*. can be better fit with the Pointer Algorithm but only by using an unrealistically large value of the persistence length of around 200 nm (in the simulation, the maximum value of l_p is set to 120 nm). The premature upturn in G'' in the data of Khatory *et al*. (1993) might be due to the large salt-surfactant concentration ratio (around 10). Or perhaps the mechanical data are unreliable at these frequencies. But, we have chosen not to force a fitting of these high-frequency data by using such an unrealistically high persistence length.

The parameter values suggested by Oelschlaeger *et al*. (2010), Khatory *et al*. (1993), and obtained from our simulations with parameters either all freely fitted [in the case of Oelschlaeger *et al*. (2010)] or d alone fixed [in both the case of Oelschlaeger *et al*. (2010) and of Khatory *et al*. (1993)] or both d and l_p fixed [in the case of Khatory *et al*. (1993)] to what we consider realistic values $\{d = 4.4\,\text{nm}$ [Nettesheim and Wagner (2007)], $l_p = 40\,\text{nm}\}$ are shown in Table VI.

In Table VI, for both data sets, an order of magnitude difference in estimated values of $\langle L \rangle$ is seen between the values reported in the literature and those we have extracted from our simulations. Some of this difference (around a factor of 2) arises because we take into account the effect of CR. However, the main reason lies in the different frequency ranges we used for predicting $\langle L \rangle$: Cates [Cates and Candau (1990)] and Granek [Granek (1994)] rely on the transition region [i.e., the ratio G''_{min}/G_N used in Eq. (18)], while our estimate comes from the low frequency region which is more sensitive to the average micelle length than is the transition region. In addition, the longer micelle length obtained from our method leads to a smaller value of ς (the longer the micelle is, the faster it breaks and the smaller is the value of ς). From the data of Oelschlaeger *et al*. (2010), by including bending modes in the simulation, the persistence length l_p and micelle diameter d can also be extracted from the high frequency behavior; the values we obtain are similar but not identical to the estimates obtained by Oelschlaeger *et al*. (2010). The difference might be the result of a larger predicted value of G_N than that for Oelschlaeger *et al*. (2010). Note also that the ratio (α_e) of l_e to l_p extracted from the data of Oelschlaeger *et al*. (2010) puts this solution close to, or in, the cross-over region

TABLE VI. Estimation of parameters for data from Oelschlaeger *et al*. (2010) and Khatory *et al*. (1993).

	Oelschlaeger *et al*. (2010)			Khatory *et al*. (1993)		
		Simulation			Simulation	
Parameters	Literature	Freely fitted	d fixed	Literature	d fixed	d, l_p fixed
G_N(Pa)	255	285	288	95	100	99
ς	—	1.13×10^{-2}	1.0×10^{-2}	0.79–1.23	1.52×10^{-2}	4.95×10^{-2}
$\langle L \rangle$(μm)	0.24	5.35	5.15	0.66	6.88	5.77
α_e	0.76	2.23	1.76	4.2	1.2	3
d (nm)	4.4	3.8	4.4	—	4.4	4.4
l_e(nm)	22.6	87	86	63.1	144	120
l_p(nm)	29.8	39	49	15	120	40

Note: Since high frequency zone is unreachable for data from Khatory *et al*. (1993), the micelle diameter cannot be estimated using our method. The value of $d = 4.4$ nm used in the simulation for this case is taken from SANS measurements [Nettesheim *et al*. (2007)].

($\alpha_e = 2.23$ and 1.76) between tight and loose entanglements, showing that our cross-over formula may be important for modeling this solution. Note also that the estimated values for l_e and l_p for data from Khatory *et al*. (1993) in the second to last column in Table VI, when only the micelle diameter d is held fixed, cannot be taken seriously since l_p reaches the maximum value ($l_p \leq 120$ nm) that our simulation allows, which is still not high enough to fit the upturn.

By fixing the micelle diameter to an experimental value, rather than allowing it to be fit, the estimation of the persistence length for the data of Oelschlaeger *et al*. (2010) changes from 39 to 49 nm, which allows a good fitting behavior at high frequencies to be maintained. The values of other parameters change only slightly, which shows the robustness of their fitted values using our method. However, if data in the high frequency region are poor or missing as is the case for the data of Khatory *et al*. (1993), estimation of other parameters will depend on the value of persistence length assumed, as shown in Table VI. Thus, the results from fitting the data of Oelschlaeger *et al*. (2010) indicate that if high frequency data are available, four of the five parameters can be extracted using our method. The fifth parameter, the micelle diameter d, must be supplied from nonrheological data, but its value is known *a priori* well enough that the other parameters can be robustly extracted from the model. However, if high frequency data are not available, or are unreliable, as appears to be the case for the data of Khatory *et al*. (1993), the persistence length must be supplied from nonrheological considerations, or else the value of ς cannot be robustly determined, as indicated by its sensitivity to the value of the persistence length shown in the last two columns of Table VI. However, the average micelle length and especially the plateau modulus G_N are seen in Table VI to be much less sensitive to an incorrect value of the persistence length l_p. A detailed analysis of the sensitivity of extracted parameter values to uncertainties in parameters or rheological data will be the focus of a later paper.

VII. CONCLUSIONS AND FINAL COMMENTS

We have developed an algorithm based on Cates' model for wormlike micelles that we believe allow more accurate rheological predictions than before. We have included additional mechanisms beyond those of Cates' model, including CR by double reptation, reptation in the tight entanglement regime as well as in the cross-over between loose and tight entanglements, and bending modes at high frequency. Based on the most up-to-date theories of polymer dynamics and innovations in modeling, fits to rheological data using our pointer algorithm allow more micelle parameters (including micelle persistence length) to be estimated, and more accurate estimates to be obtained than was possible from the earlier approaches using Cates' method. The advantages of our simulation method are illustrated by obtaining micelle parameters from fits to G' and G'' data by Oelschlaeger *et al*. (2010) over six decades of frequency with an average deviation of only 6%. We find significant differences between the best-fit micelle parameters derived from our algorithm and those obtained by the traditional method of Cates and coworkers, especially in the average micelle length, which is an order of magnitude larger than inferred from the traditional method. Future work will focus on an analysis of parameter sensitivity and the effect of CR and high frequency data on parameter estimation. It will also be worthwhile to study the effect of salt concentration, concentration of surfactant, and temperature on the parameter values extracted by our method and to compare parameter values extracted from our rheological method with those obtained more directly from electron microscopy, neutron scattering, or other methods. We note that our method

is limited to linear micelles and to linear viscoelasticity. Extension to branched micelles and nonlinear rheology is also highly desirable, but these remain as future tasks.

ACKNOWLEDGMENTS

The authors acknowledge support from NSF (under Grants CBET-0853662 and DMR 0906587) and discussions with Xueming Tang, Mike Cates, and with Mike Weaver, Peter Koening, and Shawn Mcconaughy of Procter & Gamble. Any opinions, findings, and conclusions, or recommendations expressed in this material are those of the authors and do not necessarily reflect the views of the National Science Foundation (NSF).

APPENDIX A: PREFACTOR FOR MODULUS IN LOOSE-ENTANGLEMENT REGIMES

For wormlike micelles in water, the plateau modulus (G_N) has been given by Milner (2005), which is valid for polymer chains in a good solvent

$$G_N \cong \frac{216 k_B T}{n^2 p_{Mil}^3} \phi^{\frac{9}{4}}, \tag{A1}$$

where ϕ is the volume fraction of surfactant, n is a constant determined empirically with a value of around 22.4, and p_{Mil} is the "packing length" as defined by Milner for polymer melts as

$$p_{Mil} = \frac{6 v_b}{b_K^2}, \quad \text{with } v_b = \frac{\pi}{4} d^2 b_K. \tag{A2}$$

Here, v_b is the volume of a single Kuhn step for a micelle and d is the micelle diameter. Note there is another definition of packing length, given by Fetters *et al*. (1999), which we do not use here but differs from that of Milner by a factor of 6.

Combining Eq. (A1) and Eq. (A2) yields

$$G_N \cong \frac{512 l_p^3}{\pi^3 n^2 d^6} k_B T \phi^{\frac{9}{4}}. \tag{A3}$$

The tube diameter (a) is related to the packing length (p_{Mil}) [Milner (2005)] for flexible polymers in the melt by

$$a = \frac{n p_{Mil}}{6} = \frac{n\pi}{8} \frac{d^2}{l_p}. \tag{A4}$$

In a solution with a good solvent, Eq. (A4) must be modified to

$$a = \frac{n\pi}{8} \frac{d^2}{l_p} \phi^{-3/4}. \tag{A5}$$

For loose entanglements in good solvents, the formula for d is therefore

$$d^2 = 2^{2/5} \frac{8}{n\pi} l_e^{3/5} l_p^{7/5} \phi^{3/4}. \tag{A6}$$

Combining the above equation with Eq. (A3) gives

$$G_N \cong 9.75 \frac{k_B T}{\left(l_p^{0.4} l_e^{0.6}\right)^3} = 9.75 \frac{k_B T}{\xi^3}, \tag{A7}$$

which yields the value of prefactor $A = 9.75$ used in the main text.

APPENDIX B: THE GA FOR CONVERTING TO FREQUENCY DOMAIN

The GA belongs to the family of evolutionary algorithms that provide useful solutions to multivariable optimization and searching problems [Melanie (1996)]. By mimicking the phenomenon of evolution in nature, a GA evolves an ensemble of solutions gradually toward better ones. A standard GA involves "selection," "inheritance," "crossover," and "mutation" steps. During each generation, every individual solution (which in our case is an independent set of fitting parameters) will pass through the above steps with a possibility of thereby forming a better solution. Meanwhile, some solutions will be eliminated from the ensemble because of their weak fitness (large fitting error). A detailed description of GA applied to our problem is detailed in what follows.

A. Problem setup

We first express the stress relaxation function (μ) as a summation of finite exponential functions with time constants (τ_i) and weights (μ_i)

$$\mu(t) = \sum_{i=1}^{20} \mu_i \exp(-t/\tau_i), \quad \mu_i > 0. \tag{B1}$$

Here, 20 terms are used as a compromise between computational cost and accuracy. Equation (B1) can be transformed into the frequency domain analytically as

$$G'(\omega) = G_N \sum_{i=1}^{20} \mu_i \frac{\omega^2 \tau_i^2}{1 + \omega^2 \tau_i^2}, \quad G''(\omega) = G_N \sum_{i=1}^{20} \mu_i \frac{\omega \tau_i}{1 + \omega^2 \tau_i^2}. \tag{B2}$$

Thus, the transformation problem has been converted into a nonlinear fitting problem with multiple (40) variables, and the GA yields an optimized solution for the set of constants (μ_i, τ_i), whose detailed procedure is shown below.

B. Initialization

In a GA, the initial guess is generated by randomly choosing parameter values within established ranges. For our problem, the frequency typically spans 0.01–10^6 rad/s, and $\mu(t)$ is no greater than 1, which yields ranges for the parameters of

$$\mu_i\text{: } 10^{-5} - 10^0, \quad \tau_i\text{: } 10^{-8} - 10^3. \tag{B3}$$

An outline of the initialization for our GA is presented in Fig. 22, where $N = 20$ is the number of exponential terms [Eq. (B1)] and M is the size of the solution ensemble.

According to the routine depicted by Fig. 22, the GA is initiated by an ensemble consisting of an $M \times N$ matrix with M rows of N pairs of entries (μ_i, τ_i). Each row is an independent parameter set ordered so that the larger τ_i is placed at the left side of the matrix, while each row is ordered by the fitness ε (fitting error) calculated by Eq. (B4), with smaller errors toward the top.

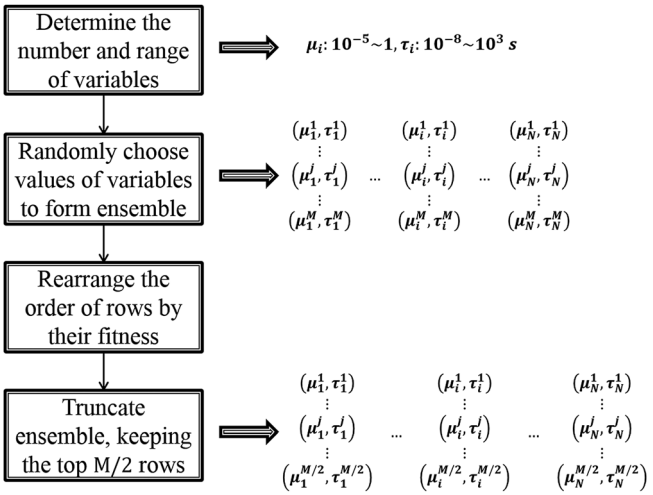

FIG. 22. The initialization of GA.

$$\varepsilon = \frac{\sum_{j=1}^{n} \left| \mu(t_j) - \sum_{i=1}^{N} \mu_i \exp\left(-t_j/\tau_i\right) \right|}{\sum_{j=1}^{n} \mu(t_j)}, \tag{B4}$$

where n is the total number of simulation data points in time domain.

After initialization, the ensemble will be truncated to half of its original size ($M/2$) for further manipulation. The truncated ensemble is called "father" generation.

C. Evolution

As illustrated in Fig. 23, after two important steps (crossover and mutation), the father generation will evolve to a "son" generation: A better ensemble with size (M) at the end of evolutionary step k. As a starting ensemble for next iteration, the son generation contains the top $M/4$ rows of the father generation with the least fitting error, and $M/2$ rows resulting from crossover and mutation (described below). The remaining $M/4$ rows are generated from the same random process used to create the initial sets of parameters. A more detailed description for crossover and mutation is given below.

1. Crossover

Comparisons are made between computer-generated random numbers and an "inheritance probability" (P_c), whose value is the probability that crossover occurs. In our case, a one-point crossover technique is used: All parameter pairs beyond a randomly selected pair are switched with the corresponding values of the neighboring row. This allows for parameters with high "fitness" in one row to be transmitted to another row, with the possibility that a superior overall fitness might arise.

2. Mutation

Similarly to crossover, we set a mutation probability (P_m), but this time for replacing a single randomly chosen parameter pair with random numbers generated from the range given by Eq. (B3). Note that crossover acts on a portion of a row, while mutation acts on a single parameter pair.

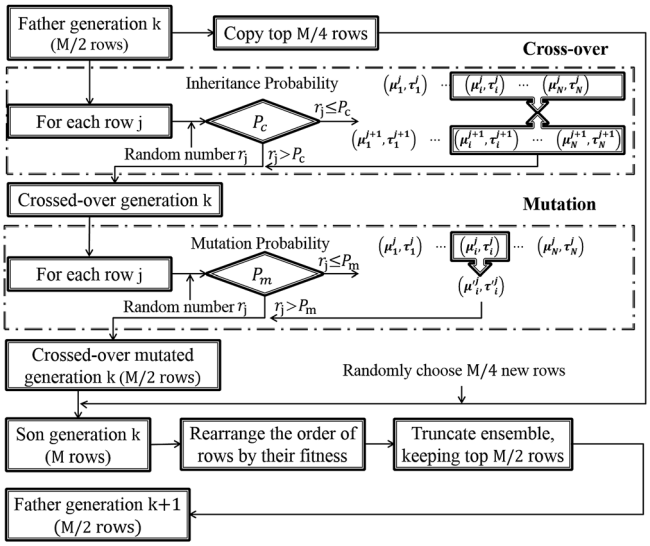

FIG. 23. Flowchart of GA.

The algorithm is continued for enough generations to find a parameter set with acceptable fitting error, which we take to be an average error of 1% per point. The transformed results are shown in Fig. 24. Based on simulation performance, we find that the optimal choices for M, P_c, and P_m are 40, 0.5, and 0.05, respectively. The CPU time of a single processor (on Intel® Core™ i5 CPU with 2.27 GHz) for fitting 500 rheological data points is around 0.5 h for 15 000 generations, which is the number of generations typically needed for convergence.

3. Constraint method

However, as ς increases, and the distribution of relaxation times becomes broader, even small fitting deviations for $\mu(t)$ at early times cause obvious "wiggles" at high frequencies in the normalized Cole-Cole plot (Fig. 25). We find that this high sensitivity to

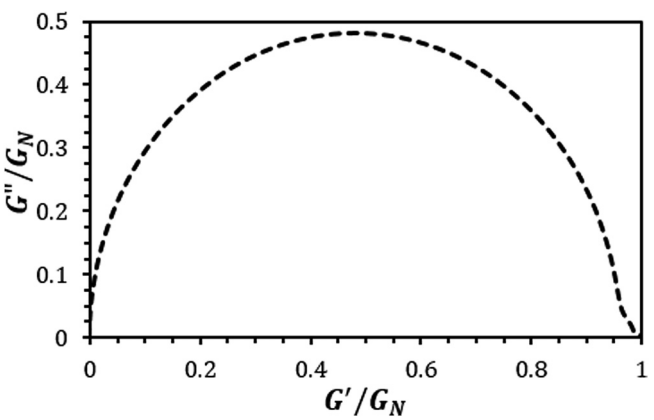

FIG. 24. Normalized Cole-Cole plot for standard values of parameters obtained from GA-aided Fourier transform.

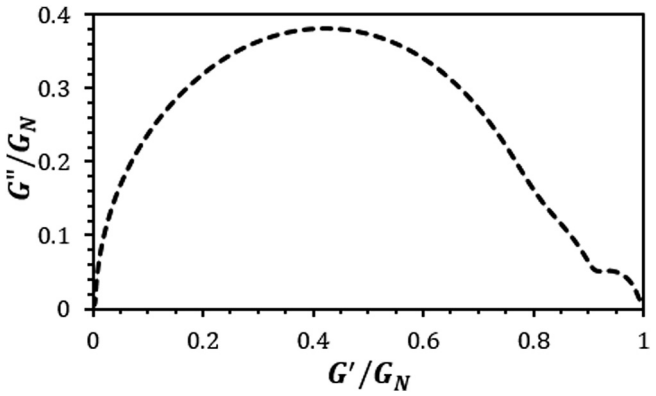

FIG. 25. The same as Fig. 24, except with $\varsigma = 0.01$.

early-time fitting results from very unevenly distributed τ_i and magnitudes of μ_i that can change by one or two orders with increasing mode number i, where i is numbered sequentially from slowest to fastest mode. Thus, modifications are needed to achieve better high-frequency behavior.

We fix the above problem using an artificial constraint that confines the ratios of neighboring μ_i values to the range 0.01–100. Although this method slightly increases the computational time, the fitness [see Eq. (B4)] is still minimized within this constraint. Since spacing values of τ_i logarithmically only works well for a wide distribution of relaxation times (large ς), a more general approach is to make each τ_i movable within an interval satisfying

$$I_{min} + \frac{I_{max} - I_{min}}{N}(i-1) < \log(\tau_i) < I_{min} + \frac{I_{max} - I_{min}}{N} i, \tag{B5}$$

where I_{max} and I_{min} are the maximum and minimum values for $\log(\tau_i)$, respectively. $N = 20$ is the total number of modes. For our case [$\tau_i : 10^{-8} - 10^3$s, see Eq. (B3)], we have $I_{max} = 3, I_{min} = -8$.

The advantage of setting boundaries for each τ_i is that for different values of ς, each τ_i can slide within its interval to obtain the best fit for the stress relaxation function $\mu(t)$. Using standard values of parameters except for $\varsigma = 0.01$, transformation results with the constraint method are given in Fig. 26.

APPENDIX C: SIMULATION TESTING DETAILS

A. Equilibrium distribution

The random breakage/rejoining within the pointer algorithm produces a simulated micelle length distribution that matches the theoretical equilibrium one [Eq. (15)] after fluctuations are averaged out ($R^2 = 0.97$) over a simulation time of duration ten times the terminal relaxation, $10\bar{\tau} \sim 10\bar{\tau}_{rep}\varsigma^{0.62}$ (see Table IV for the scaling of relaxation time with ς), which in computer time is typically half a day for a single Intel® Core™ i5 CPU with 2.27 GHz.

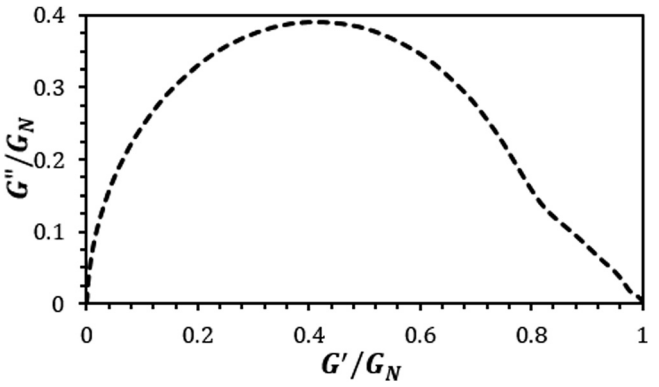

FIG. 26. The same as Fig. 25, except that a constraint method is used.

B. Pure reptation

To test that the simulation correctly accounts for reptation, we turn off all the other mechanisms and simulate a set of chains with the same length. The results of simulation compare favorably ($R^2 = 0.98$) with the theoretical ones from the Doi-Edwards theory [Eq. (13)], indicating that our simulation method captures reptation properly.

C. Reptation and CLFs

Next, we add CLFs to pure reptation, again simulating with a monodisperse ensemble of chains. We find that our simulation results are close to ($R^2 = 0.96$) the theoretical prediction for a single-mode relaxation, whose reptation time is corrected by CLFs, according to Eq. (21) from Likhtman and McLeish (2002). As shown in Fig. 27, the rather small deviations are concentrated at early times, where the single-mode description of CLFs given by Eq. (21) is not expected to work perfectly, and relaxation is somewhat faster than predicted by Eq. (21). Thus, since CLFs introduce additional fast modes, the deviation between this theory and the simulations seen at early times is expected and does not

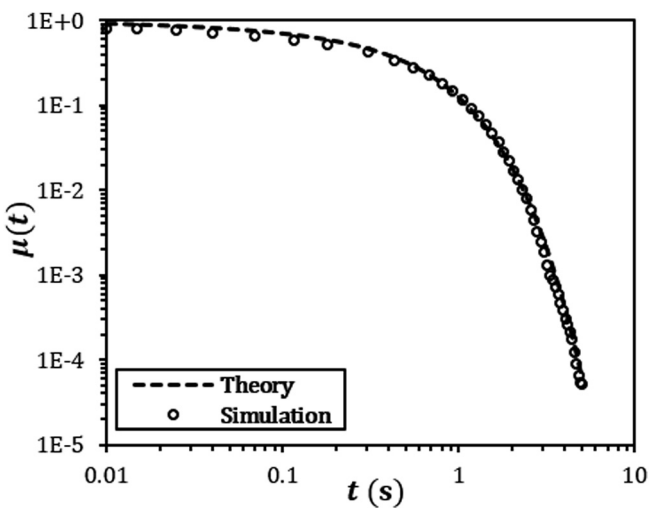

FIG. 27. Relaxation function with CLFs and reptation for monodisperse ensemble for $Z = 33.5, \tau_{rep} = 1s,\ \alpha_e = 2,\ l_p = 30\,\text{nm},$ and $d = 3\,\text{nm}$. The "Theory" here is the single-mode relaxation expression given by Eq. (21).

necessarily reflect inaccuracy in the simulations. In addition, at very long times where the unrelaxed fraction μ falls below 0.1%, our treatment on CLFs [Eq. (40)] overestimates the rate of relaxation. Thus, when relaxation is nearly complete and μ reaches 0.1%, we simply switch off CLFs, which is reasonable since its effect is negligible at such late times.

D. Convergence

To obtain convergence with time step, we need to modify the simulation time step from that given in Eq. (38) to

$$\Delta t = \min\left[\frac{\bar{\tau}_{br}}{2 \cdot num}, \Delta t_L\right], \quad \Delta t_L \sim O\left(\frac{\bar{\tau}_{rep}}{\langle L\rangle^3}\right) , \tag{C1}$$

where Δt_L is a time constant with units of seconds. The reason for preventing the time step from becoming larger than Δt_L lies in the convergence requirement when other mechanisms (reptation, CLFs) become important, as ς (and thus $\bar{\tau}_{br}$) becomes larger. We find empirically that $\Delta t_L = 10^{-6}$s fits most of our convergence requirements. This criterion no doubt depends on our simulation of aqueous systems and is likely set by the shortest relaxation time of micelles in the ensemble.

In each run, 10 000 micelles were simulated out to a time at which the relaxation function $\mu(t)$ has relaxed from unity to 0.001. To be sure that a run of this duration is sufficient to average out noise, we compared results from a single such run to those obtained by averaging over, 5 and 10 such runs, and found one such run to be sufficient to obtain reproducible rheological properties. Thus, our pointer algorithm simulation successfully captures the living feature of wormlike micelles with convergence with respect to time step, run duration, and size of ensemble.

APPENDIX D: COLE-COLE PLOTS FOR A WIDE RANGE OF ς AND $\bar{Z}_t$

As described in the text, we obtain normalized Cole-Cole plots for a range of ς and $\bar{Z}_t$, which are presented in Figs. 28 and 29. These plots were used to obtain the correlations discussed in the text.

APPENDIX E: DETAILED EXPRESSION FOR $\bar{Z}_t$, $\bar{\tau}_{rep}$, G_N, AND $G^H(\omega)$

The detailed functional forms for Eqs. (44b) and (44c) are as follows.

For the average number of entanglements per tube, by combining Eqs. (2), (9), and (28), we obtain

$$\bar{Z}_t = \frac{\langle L\rangle}{\alpha_e l_p \cdot \max[\sqrt{0.5\alpha_e},\ 1]} . \tag{E1}$$

To obtain $\bar{\tau}_{rep}$, combining Eqs. (4), (12), and (28), gives

$$\bar{\tau}_{rep} = \frac{2}{\pi}\frac{\eta_s}{k_B T \ln(\alpha_e^{0.6} l_p/d)}\frac{\langle L\rangle^3}{\{\max[\sqrt{0.5\alpha_e},\ 1]\}^2} . \tag{E2}$$

For G_N, we use Eq. (32)

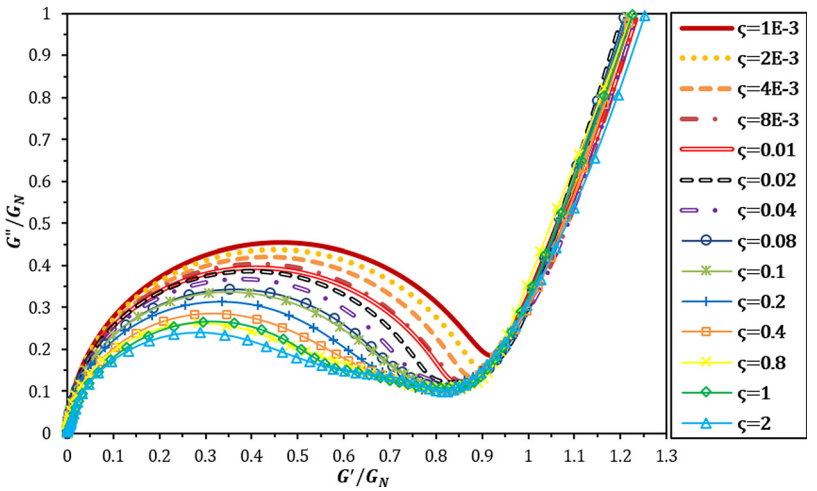

FIG. 28. Family of normalized Cole-Cole plots for different values of ς with standard values of other parameters.

$$G_N = \frac{\alpha_e^3}{\alpha_e^3+3}\cdot 9.75\frac{k_BT}{\alpha_e^{9/5}l_p^3}+\frac{3}{\alpha_e^3+3}\cdot\frac{28}{5\pi}\frac{\phi k_BT}{d^2\alpha_e l_p}. \tag{E3}$$

Finally, according to Eqs. (33) and (34), a detailed expression for Eq. (44c) is also given here

$$G^H(\omega) = \frac{4(2i)^{3/4}}{15\pi}(k_BT)^{1/4}\phi\left[\frac{4\pi\eta_s}{\ln(0.6\alpha_e^{0.6}l_p/d)}\right]^{3/4}\cdot\frac{l_p^{5/4}\omega^{3/4}}{d^2}+i\omega\eta_s. \tag{E4}$$

The definitions of all above parameters are the same as in the main text.

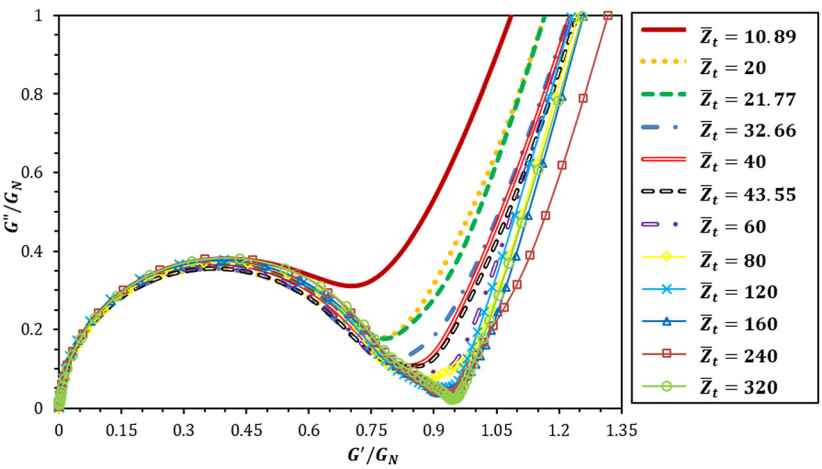

FIG. 29. Family of normalized Cole-Cole plots for different values of $\bar{Z}_t$ with standard values of other parameters.

References

Appell, J., G. Porte, and Y. Poggi, "Quantitative estimate of the orientational persistence length of flexible elongated micelles of cetylpyridinium bromide," J. Colloid Interface Sci. **87**, 492–499 (1982).

Appell, J., and J. Marignan, "Structure of giant micelles—A small-angle neutron-scattering study," J. Phys. II France **1**, 1447–1454 (1991).

Batchelor, G. K., "The stress generated in a non-dilute suspension of elongated particles by pure straining motion," J. Fluid Mech. **46**, 813–829 (1971).

Brown, W., K. Johansson, and M. Almgren, "Threadlike micelles from cetyltrimethyl-ammonium bromide in aqueous sodium naphthalenesulfonate solutions studied by static and dynamic light scattering," J. Phys. Chem. **93**, 5888–5894 (1989).

Bruce, C. D., M. L. Berkowitz, L. Perera, and M. D. Forbes, "Molecular dynamics simulation of sodium dodecyl sulfate micelle in water," J. Phys. Chem. B **106**, 3788–3793 (2002).

Candau, S. J., A. Khatory, F. Lequeux, and F. Kern, "Rheological behavior of wormlike micelles: Effect of salt content," J. Phys. IV France **3**, 197–209 (1993).

Candau, S. J., E. Hirsch, and R. Zana, "Rheological properties of semidilute and concentrated aqueous solutions of cetyltrimethylammonium bromide in the presence of potassium bromide," Langmuir **5**, 1225–1229 (1989).

Cates, M. E., "Reptation of living polymers: Dynamics of entangled polymers in the presence of reversible chain-scission reactions," Macromolecules **20**, 2289–2296 (1987).

Cates, M. E., "Dynamics of living polymers and flexible surfactant micelles: Scaling laws for dilution," J. Phys. **49**, 1593–1600 (1988).

Cates, M. E., and S. J. Candau, "Statics and dynamics of worm-like surfactant micelles," J. Phys.: Cond. Matter **2**, 6869–6892 (1990).

Clausen, T. M., P. K. Vinson, J. R. Minter, H. T. Davis, Y. Talmon, and W. G. Miller, "Viscoelastic micellar solutions: Microscopy and rheology," J. Phys. Chem. **96**, 474–484 (1992).

Couillet, I., T. Hughes, G. Maitland, F. Candau, and S. J. Candau, "Growth and scission energy of wormlike micelles formed by a cationic surfactant with long unsaturated tails," Langmuir **20**, 9541–9550 (2004).

Croce, V., T. Cosgrove, G. Maitland, T. Hughes, and G. Karlsson, "Rheology, cryogenic transmission electron spectroscopy and small-angle neutron scattering of highly viscoelastic wormlike micellar solutions," Langmuir **19**, 8536–8541 (2003).

de Gennes, P. G., *Scaling Concepts in Polymer Physics* (Cornell University Press, Ithaca, New York, 1979).

Dealy, J. M., and R. G. Larson, *Structure and Rheology of Molten Polymers: From Structure to Flow Behavior and Back Again* (Hanser Gardner, Cincinnati, 2005).

Decruppe, J. P. F., and S. Lerouge, "A comparison of some rheophysical properties of cetyltrimethylammonium bromide/H_2O and cetyltrimethylammonium bromide/D_2O solutions," J. Colloid Polym. Sci. **277**, 891–894 (1999).

des Cloizeaux, J., "Double reptation vs. simple reptation in polymer melts," Europhys. Lett. **5**, 437–442 (1988).

Doi, M., and S. F. Edwards, *The Theory of Polymer Dynamics* (Clarendon, Oxford, 1986).

Fetters, L. J., D. J. Lohse, and W. W. Graessley, "Chain dimensions and entanglement spacings in dense macromolecular systems," J. Polym. Sci. B: Polym. Phys. **37**, 1023–1033 (1999).

Galvan-Miyoshi, J., J. Delgado, and R. Castillo, "Diffusing wave spectroscopy in Maxwellian fluids," Eur. Phys. J. E **26**, 369–377 (2008).

Gamez-Corrales, R., J. F. Berret, L. M. Walker, and J. Oberdisse, "Shear-thickening dilute surfactant solutions: Equilibrium structure as studies by small-angle neutron scattering," Langmuir **15**, 6755–6763 (1999).

Gittes, F., and F. C. MacKintosh, "Dynamic shear modulus of a semiflexible polymer network," Phys. Rev. E **58**, 1241–1244 (1998).

Gomez, E. S., D. L. Diaz, and R. Castillo, "Microrheology and characteristic lengths in wormlike micelles made of a zwitterionic surfactant and SDS in brine," J. Phys. Chem. B **114**, 12193–12202 (2010).

Granek, R., "Dip in $G''(\omega)$ of polymer melts and semidilute solutions," Langmuir **10**, 1627–1629 (1994).

Granek, R., and M. E. Cates, "Stress relaxation in living polymers: Results from a Poisson renewal model," J. Chem. Phys. **96**, 4758–4767 (1992).

Grmela, M., F. Chinesta, and A. Ammar, "Mesoscopic tube model of fluids composed of worm-like micelles," J. Rheol. Acta **49**, 495–506 (2010).

Hassan, P. A., S. J. Candau, F. Kern, and C. Manohar, "Rheology of wormlike micelles with varying hydrophobicity of the counterion," Langmuir **14**, 6025–6029 (1998).

Helgeson, M. E., T. K. Hodgdon, E. W. Kaler, and N. J. Wagner, "A systematic study of equilibrium structure, thermodynamics, and rheology of aqueous CTAB/$NaNO_3$ wormlike micelles," J. Colloid Interface Sci. **349**, 1–12 (2010).

Heo, Y., and R. G. Larson, "The scaling of zero-shear viscosities of semidilute polymer solutions with concentration," J. Rheol. **49**, 1117–1128 (2005).

Ilgenfritz, G., R. Schneider, E. Grell, E. Lewitzki, and H. Ruf, "Thermodynamic and kinetic study of the sphere-to-rod transition in nonionic micelles: Aggregation and stress relaxation in $C_{14}E_{18}$ and $C_{16}E_8/H_2O$ system," Langmuir **20**, 1620–1630 (2004).

Imae, T., "Light scattering of spinnable, viscoelastic solutions of hexadecyltrimethylammonium salicylate," J. Phys. Chem. **94**, 5953–5959 (1990).

Imae, T., and S. Ikeda, "Sphere-rod transition of micelles of tetradecyltrimethylammonium halides in aqueous sodium halide solutions and flexibility and entanglement of long rodlike," J. Phys. Chem. **90**, 5216–5223 (1986).

Jusufi, A., A. P. Hynninen, and A. Z. Panagiotopoulos, "Implicit solvent models for micellezation of ionic surfactants," J. Chem. Phys. B **112**, 13783–13792 (2008).

Khatory, A., F. Lequeux, F. Kern, and S. J. Candau, "Linear and nonlinear viscoelasticity of semidilute solutions of wormlike micelles at high salt content," Langmuir **9**, 1456–1464 (1993).

Kuperkar, K., L. Abezgauz, D. Danino, G. Verma, P. A. Hassan, V. K. Aswal, D. Varade, and P. Bahadur, "Viscoelastic micellar water/CTAB/$NaNO_3$ solution: Rheology, SANS and cryo-TEM analysis," J. Colloid Interface Sci. **323**, 403–409 (2008).

Larson, R. G., "The lengths of thread-like micelles inferred from rheology," J. Rheol. **56**, 1363–1374 (2012).

Larson, R. G., T. Sridhar, L. G. Leal, G. H. McKinley, A. E. Likhtman, and T. C. McLeish, "Definition of entanglement spacing and time constants in the tube model," J. Rheol. **47**, 809–818 (2003).

Lequeux, F., "Reptation of connected wormlike micelles," Europhys. Lett. **19**, 675–681 (1992).

Lequeux, F., "Structure and rheology of wormlike micelles," Colloid Interface Sci. **1**, 341–344 (1996).

Likhtman, A. E., and T. C. McLeish, "Quantitative theory for linear dynamics of linear entangled polymers," Marcomolecules **35**, 6332–6343 (2002).

Magid, L. J., Z. Han, Z. Lin, and P. D. Butler, "Tuning the contour lengths and persistence lengths of cationic micelles: The role of electrostatics and specific ion binding," J. Phys. Chem. B **104**, 6717–6727 (2000).

Marignan, J., J. Appell, P. Bassereau, G. Porte, and R. P. May, "Local structures of the surfactant aggregates in dilute-solutions deduced from small-angle neutron-scattering patterns," J. Phys. **50**, 3553–3566 (1989).

Melanie, M., *An Introduction to Genetic Algorithms* (MIT, Cambridge, 1996).

Michels, B., and G. Waton, "Effect of pentanol and salt on the fusion-scission kinetics for CTAB micelles," J. Phys. Chem. A **107**, 1133–1137 (2003).

Milner, S. T., "Predicting the tube diameter in melts and solutions," Macromolecules **38**, 4929–4939 (2005).

Milner, S. T., and T. C. McLeish, "Reptation and contour-length fluctuations in melts of linear polymers," Phys. Rev. Lett. **81**, 725–728 (1998).

Morse, D. C., "Viscoelasticity of concentrated isotropic solutions of semiflexible polymers: 1. Model and stress tensor," Macromolecules **31**, 7030–7043 (1998a).

Morse, D. C., "Viscoelasticity of concentrated isotropic solutions of semiflexible polymers: 2. Linear response," Macromolecules **31**, 7044–7067 (1998b).

Nagarajan, R., "Association of nonionic polymers with micelles, bilayers, and microemulsions," J. Chem. Phys. **90**, 1980–1994 (1989).

Nemoto, N., M. Kuwahara, M. Yao, and K. Osaki, "Dynamic light scattering of CTAB/NaSal threadlike micelles in a semidilute regime. 3. Dynamical coupling between concentration fluctuation and stress," Langmuir **11**, 30–36 (1995).

Nettesheim, F., and N. J. Wagner, "Fast dynamics of wormlike micellar solutions," Langmuir **23**, 5267–5269 (2007).

Oelschlaeger, C., M. Schopferer, F. Scheffold, and N. Willenbacher, "Linear-to-branched micelles transition: A rheometry and diffusing wave spectroscopy (DWS) study," Langmuir **25**, 716–723 (2009).

Oelschlaeger, C., P. Suwita, and N. Willenbacher, "Effect of counterion binding efficiency on structure and dynamics of wormlike micelles," Langmuir **26**, 7045–7053 (2010).

Pasquali, M., V. Shankar, and D. C. Morse, "Viscoelasticity of dilute solutions of semi-flexible polymers," Phys. Rev. E **64**, 020802 (2001).

Porte, G., J. Appell, and Y. Poggi, "Experimental investigation on the flexibility of elongated cetylpyridinium bromide micelles," J. Phys. Chem. **84**, 3105–3110 (1980).

Rosen, M. J., *Surfactants and Interfacial Phenomena*, 2nd ed. (Wiley, New York, 1989).

Rothstein, J. P., "Transient extensional rheology of wormlike micelle solutions," J. Rheol. **47**, 1227–1247 (2003).

Schubert, B. A., E. W. Kaler, and N. J. Wagner, "The microstructure and rheology of mixed cationic/anionic wormlike micelles," Langmuir **19**, 4079–4089 (2003).

Shang, B. Z., Z. Wang, and R. G. Larson, "Effect of headgroup size, charge, and solvent structure on polymer-micelle interactions, studied by molecular dynamics simulation," J. Phys. Chem. B **113**, 15170–15180 (2009).

Shikata, T., S. J. Dahman, and D. S. Pearson, "Rheo-optical behavior of wormlike micelles," Langmuir **10**, 3470–3476 (1994).

Siriwatwechakul, W., T. LaFleur, R. K. Prudhomme, and P. Sullivan, "Effects of organic solvents on the scission energy of rodlike micelles," Langmuir **20**, 8970–8974 (2004).

Terech, P., V. Schaffhauser, P. Maldivi, and J. M. Guenet, "Living polymers in organic solvents," Langmuir **8**, 2104–2106 (1992).

Tsenoglou, C., "Molecular-weight polydispersity effects on the viscoelasticity of entangled linear-polymers," Macromolecules **24**, 1762–1767 (1991).

Tuminello, W. H., "Molecular-weight polydispersity effects on the viscoelasticity of entangled linear polymers," Polym. Eng. Sci. **26**, 1339–1347 (1986).

Tuner, M. S., and M. E. Cates, "Linear viscoelasticity of living polymers: A quantitative probe of chemical relaxation times," Langmuir **7**, 1590–1594 (1991).

Tuner, M. S., and M. E. Cates, "Linear viscoelasticity of wormlike micelles: A comparison of micellar reaction kinetics," J. Phys. France **2**, 503–519 (1992).

van der Schoot, P., and J. P. Wittmer, "Linear aggregation revisited: Rods, rings and worms," Macromol. Theory Simul. **8**, 428–432 (1999).

Wang, Z., and R. G. Larson, "Molecular dynamics simulations of threadlike cetyltrimethyl-ammonium chloride micelles: Effects of sodium chloride and sodium salicylate salts," J. Phys. Chem. B **113**, 13697–13710 (2009).

Wang, Z., X. Chen, and R. G. Larson, "Comparing tube models for predicting the linear rheology of branched polymer melts," J. Rheol. **54**, 223–260 (2010).

Willenbacher, N., C. Oelschlaeger, M. Schopferer, P. Fischer, F. Cardinaux, and F. Scheffold, "Broad bandwidth optical and mechanical rheometry of wormlike micelle solutions," Phys. Rev. Lett. **99**, 068302 (2007).

Wittmer, J. P., A. Milchev, and M. E. Cates, "Dynamics Monte Carlo study of equilibrium polymers: Static properties," J. Chem. Phys. **109**, 834–844 (1998).